CIAMTIS

U.S. DOT Region 3 University Transportation Center

Efficient Service Life Extension of Bridges through Risk-based Lifecycle Management and High-performance Construction Materials: Emphasis on Corrosion-resistant Steel

September 30, 2020

Prepared by:

Dan M. Frangopol, David Y. Yang, and Xu Han

Advanced Technology for Large Structural Systems (ATLSS) Engineering Research Center, Lehigh University

r3utc.psu.edu

PennState College of Engineering

LARSON TRANSPORTATION INSTITUTE

DISCLAIMER

Technical Report Documentation Page

1. Report No.	2. Government Accession No.	3. Recipient's Catalog No.
CIAM-UTC-REG6		

4. Title and Subtitle	5. Report Date
Efficient Service Life Extension of Bridges through Risk-based Lifecycle Management and High-performance Construction Materials: Emphasis on Corrosion-resistant Steel	September 30, 2020
	6. Performing Organization Code

7. Author(s)	8. Performing Organization Report No.
Dan M. Frangopol, https://orcid.org/0000-0002-9213-0683 David Y. Yang, and Xu Han	

9. Performing Organization Name and Address	10. Work Unit No. (TRAIS)
ATLSS Engineering Research Center Department of Civil and Environmental Engineering Lehigh University 117 ATLSS Drive Bethlehem, PA 18015	**11. Contract or Grant No.** 69A3551847103

12. Sponsoring Agency Name and Address	13. Type of Report and Period Covered
U.S. Department of Transportation Research and Innovative Technology Administration 3rd Fl, East Bldg E33-461 1200 New Jersey Ave, SE Washington, DC 20590	Final Report 02/11/2019 – 09/30/2020
	14. Sponsoring Agency Code

15. Supplementary Notes

Work funded through The Pennsylvania State University through the University Transportation Center Grant Agreement, Grant No. 69A3551847103.

16. Abstract

Corrosion is responsible for structural deterioration of a large number of steel bridges. It can considerably compromise the safety and serviceability of bridges. Inspection and maintenance of corroded structures can lead to huge direct economic cost to bridge owners and significant indirect social and environmental consequences such as traffic delays and extra greenhouse gas emissions. In this project, an effective lifecycle bridge management framework is established for novel maintenance actions based on high-performance construction materials. To counteract the detrimental effects of steel corrosion, the application of high-performance construction materials emphasizes the use of A709-50CR (formerly known as A1010), a corrosion-resistant steel locally sourced in Pennsylvania. This project focuses on steel girder bridges, which are one of the most commonly used structural forms in Pennsylvania and other Region 3 states. In order to establish the overall lifecycle management framework, the project investigated and modeled the corrosion behaviors of both conventional carbon steel and A709-50CR. To ensure that the use of A709-50CR will not exert negative impacts on the environment, a comprehensive lifecycle environmental assessment was conducted to compare carbon steel and A709-50CR bridge girders. A risk-based approach was established to minimize the lifecycle maintenance cost while controlling the lifecycle risks of deteriorating bridges. By applying this approach to A709-50CR-based maintenance actions, this project investigated the use of A709-50CR girders to replace corroded carbon steel girders in aging multi-girder steel bridges. The results indicate that using A709-50CR in such major maintenance actions can achieve considerable economic and sustainability benefits. By exploring this cost-effective application of A709-50CR, the results of this project have the potential to positively impact the current practice of bridge maintenance and significantly extend the service life of steel bridges.

17. Key Words	18. Distribution Statement
Innovative materials (A709-50CR), life\cycle assessment, maintenance optimization, durability, corrosion, steel bridges	No restrictions. This document is available from the National Technical Information Service, Springfield, VA 22161

19. Security Classif. (of this report)	20. Security Classif. (of this page)	21. No. of Pages	22. Price
Unclassified	Unclassified	55	

Table of Contents

List of Figures

List of Tables

CHAPTER 1

Introduction

BACKGROUND

Structural deterioration of aging bridges is a major problem faced by the owners and managers of transportation assets. According to the latest report card by the American Society of Civil Engineers (ASCE, 2017), one in eleven bridges in the nation is rated "structurally deficient." The situation is even more dire in USDOT Region 3 states, including Delaware, District of Columbia, Maryland, Pennsylvania, Virginia, and West Virginia. In Pennsylvania, a state with the ninth largest bridge inventory in the nation, the most recent state report card rated D+ for bridges in the state, much lower than the national average (C+); 18.34% (4,173 bridges) are in a "structurally deficient" state. The severity of the deterioration problem, compounded by the sheer amount of deficient bridges, requires that innovative intervention actions be taken for critical bridges at the most appropriate points-in-time during their service life.

For steel bridges, corrosion is one of the dominant deterioration mechanisms. Corrosion can reduce the effective thickness of steel plates, resulting in premature yielding or buckling of steel members that can drastically compromise structural safety. In addition, the buildup of corrosion products may adversely affect the functionality of bridges as the accumulated rust fills up the void space near bridge bearings or expansion joints, thereby resulting in unintended stresses in bridges. Therefore, when located in a corrosive environment (e.g., a coastal environment or under direct exposure to deicing salts), steel bridges made of carbon steel require frequent inspection and maintenance. This leads to huge direct maintenance costs and indirect social and environmental consequences such as traffic delays and extra greenhouse gas emissions.

OBJECTIVES AND SCOPE

The main goal of this project was to establish an effective lifecycle bridge management framework for novel maintenance actions based on high-performance construction materials. To counteract the detrimental effects of steel corrosion, the application of high-performance construction materials will emphasize the use of corrosion-resistant steel, a material locally available in Pennsylvania. This steel, referred to as A709-50CR (formerly known as A1010), is an innovative, low-cost stainless steel developed and produced by ArcelorMittal, a Pennsylvania-based steel manufacturer. Specifically, the objectives of this project were:

(a) to investigate and model the corrosion behaviors of both conventional carbon steel and corrosion-resistant steel,
(b) to evaluate the lifecycle cost and lifecycle environmental impact of steel bridges with conventional carbon steel and corrosion-resistant steel,
(c) to assess the lifecycle risk of steel girder bridges repaired with A709-50CR, and
(d) to conduct risk-based lifecycle maintenance optimization under uncertainty.

The project focused on steel girder bridges, which are one of the most commonly used structural forms in Pennsylvania and other Region 3 states. By devising cost-effective approaches to applying corrosion-resistant steel, the results of this project have the potential to positively impact the current practice of bridge management and significantly improve the durability and service life of deteriorating steel bridges.

CHAPTER 2

Corrosion of Steel Bridges

CORROSION AND CORROSION PROTECTION

Corrosion is an electrochemical process in which electrons are transported from an anode (an electropositive region) to a cathode (an electronegative region), which leads to the degradation of the anode and the formation of corrosion products adhering to the steel surface (NACE International, 2012). For steel bridges, corrosion can lead to the reduction of effective plate thickness. This will then in turn compromise structural safety and serviceability due to premature yielding or buckling of steel members as well as unexpected overstress attributed to the buildup of corrosion products at bridge bearings or expansion joints.

Traditionally, a coating is applied on the surface of carbon steel plates for corrosion protection. For several decades, lead-containing alkyd paint was widely used on steel bridges. It functions as a barrier to moisture and other corrosion inducers (Kogler, 2015). Alternatively, a metal more electrochemically active than iron (e.g., zinc) can be applied on steel surfaces in a process called galvanization to serve as both a barrier and a sacrificial anode to prevent corrosion of steel (Kogler, 2015). Currently, a tri-layer, zinc-rich coating system containing a zinc-rich primer base layer topped with epoxy and polyurethane layers has overtaken lead-containing alkyd paint as the most widely used coating system (Kogler, 2015). The zinc-rich primer, acting similarly to a galvanization layer, serves as the main corrosion protection component. The epoxy layer in the middle provides a barrier to moisture, and the polyurethane top layer provides an additional moisture barrier and can preserve color and gloss (Kogler, 2015). Nonetheless, regardless of the coating system used, the corrosion protection measure has only a finite lifespan in aggressive environments. Therefore, the coating system must be applied repetitively in the course of the service life.

Alternatively, bridges can be constructed using durability-enhancing materials. One example of these materials is weathering steel that has been widely used for bridge construction. In low-moisture corrosive environments, weathering steel can gradually form a protective oxide or oxy-hydroxide layer on the surface, resulting in retarded corrosion development and better durability. However, in highly corrosive and saline environments, weathering steel may fail to develop the protective layer, as the corrosion products can change from nanophase goethite (α-FeOOH) to akaganeite (β-FeOOH) and maghemite ($FeO{\cdot}Fe_2O_3$) (Groshek, 2017).

A709-50CR: A NOVAL TYPE OF STAINLESS STEEL

For moderate and severe exposure conditions, various types of stainless steel have been developed and proposed for construction applications. In this report, the application of a novel type of stainless steel, A709-50CR (formerly known as A1010), is studied. Stainless steel is a metallic alloy exhibiting high corrosion resistance. The high corrosion resistance of stainless steel is mainly attributed to the chromium content, with a further enhancement due to the addition of molybdenum and nitrogen (Daghash & Ozbulut, 2017).

Nickel is another important chemical element in stainless steel to promote the formation of austenite (FHWA, 2011). Generally, stainless steel can be divided into five main groups (Cobb, 1999). The first four groups—austenitic, ferritic, martensitic, and duplex stainless steels—are classified based on crystalline structures; the fifth group, known as precipitation hardening steel, is an alloy combining high strength and hardness with no specific crystalline structure (Cobb, 1999). Among the first four groups of stainless steel, austenitic stainless steel, characterized by around 17% chromium and from 8% to 13% nickel (Daghash & Ozbulut, 2017), is nonmagnetic and has an excellent formability in the annealed condition and a high material strength in an elevated temperature up to 500 °C (X. Q. Wang et al., 2014). Ferritic stainless steel, with a chromium content from 11% to 27% and almost zero amount of nickel (Cobb, 1999), is magnetic but has a low toughness at high temperatures (400 °C to 900 °C) (Wright, 1980). Martensitic stainless steel, usually containing 11% to 18% chromium and null to trace amounts of nickel and other elements, is magnetic and often used after hardening and tempering processes; duplex stainless steel, with 18% to 29% chromium and 3% to 8% nickel, exhibits an annealed structure consisting of about equal parts of ferrite and austenite (Cobb, 1999).

A709-50CR was originally produced in the United States by ArcelorMittal Global R&D, a steel manufacturer based in Pennsylvania, as a lower-cost alternative to duplex stainless steel while preserving its desirable characteristics such as high strength, sufficient toughness, and adequate weldability (FHWA, 2011; Groshek, 2017). A709-50CR exhibits a dual-phase microstructure consisting of both ferrite and martensite. It usually has a chromium content ranging from 10.5% to 12.5% and a maximum of 1.5% nickel content (Groshek, 2017). During A709-50CR production, the rolled steel is heated above the critical temperature for a specific grade of steel and then naturally cooled to room temperature in a process called normalizing. A tempering process then follows to achieve the target strength and hardness.

The first bridge using A709-50CR was opened to traffic in 2004 in Colusa County, California. The Glen-Colusa Canal bridge is one of California's Innovative Bridge Research and Construction Program projects. Due to the high corrosion resistance of A709-50CR, there is no need to paint the steel girders. Since then, application of A709-50CR for bridge construction has gained momentum. In 2012, a steel girder bridge was constructed in Coatesville, Pennsylvania to withstand corrosion induced by deicing salt. Two more bridges were constructed and opened to public use in Oregon in 2012 and 2013, respectively. More recently in 2016, the Virginia Department of Transportation decided to use A709-50CR for a new bridge to replace an 84-year-old bridge over the South River. The project was completed in 2017. Up to 2019, A709-50CR has been used in the construction of six bridges in the United States and two bridges in Canada (Provines et al., 2019).

CORROSION BEHAVIORS OF CARBON STEEL AND A709-50CR

Corrosion Data

For carbon steel, the corrosion product is primarily ferritic oxide (Fe_2O_3), which eventually spalls off the steel surface due to its large molecular size (Groshek, 2017). For A709-50CR (or stainless steel in general), chromium in its composition can oxidize and form a passive layer when exposed to the atmosphere, thereby preventing the forming of ferritic oxide (i.e., rusting) (Groshek, 2017).

To test the corrosion resistance of A709-50CR under immersive conditions, the Federal Highway Administration (FHWA, 2011) conducted a cyclic corrosion test (CCT) based on the Society of Automotive Engineers (SAE) J2334 standard (SAE J2334, 1998). In the test, the concentration of NaCl in the original SAE J2334 solution was raised to 5% in weight to simulate the high chloride deposition at adverse locations such as under the bridge. Another solution with 3% NaCl was also prepared for comparison. Groshek (2017) repeated this CCT of A709-50CR using 5% NaCl solution and obtained a similar corrosion rate as those obtained by FHWA (FHWA, 2011). Ebrahimi et al. (2018) conducted potentiodynamic polarization testing on A709-50CR specimens using 1.5% NaCl solution.

For atmospheric corrosion, FHWA (2011) conducted field tests on A709-50CR at the Moore Drive Bridge over I-394S in Rochester, New York. Tests on other types of stainless steel similar in composition to A709-50CR have also been conducted. For instance, Kucera and Mattson (1982) provided values of annual corrosion rates of AISI 410 (a typical martensitic stainless steel with chromium composition similar to that in A709-50CR) in rural, urban, and marine environments using the wire-on-bolt technique. Southwell and Bultman (1975) conducted atmospheric corrosion tests on AISI 410 specimens used in the Miraflores Locks of the Panama Canal (located in an inland atmospheric environment) and the roof of the Washington Hotel by Limon Bay, Panama (located in a marine atmospheric environment). In an effort to investigate the impact of chromium content on the corrosion resistance of stainless steel, 101.6 mm × 152.4 mm (4 in × 6 in) steel plates with a chromium content ranging from 0.5% to 28% were exposed to the atmosphere in Newark, New Jersey (industrial); South Bend, Pennsylvania (semirural); and the testing lots located 250 m (moderate marine) away from Kure Beach, North Carolina (Schmitt & Mullen, 1968). Focusing on atmospheric corrosion, the test results of carbon steel and stainless steel are summarized in Table 2.1 and Table 2.2, respectively.

Table 2.1 Corrosion rate data of carbon steel plates

Steel Name	Exposure Condition	Corrosion Rates (μm/year)
Mild steel	Marine	36[a]
Mild steel	Marine (roof of Washington Hotel by the shore of Limon Bay)	12[b]
Unalloyed carbon steel (Cu 0.03 to 0.10 %, P < 0.07 %)	Kure Beach (250-m lot), North Carolina (eastern marine)	21.7[c]
	Point Reyes, California (western marine)	11.9[c]
Mild steel	Barcelona	20.4[d]
	Cadiz	12.5[d]
	Cabo Negro	45.3[d]
	Alicante (30-m lot)	48.3[d]
	Alicante (100-m lot)	8.4[d]
Carbon No.45	Block Island, Rhode Island	242.7[e]
	Kure Beach (250-m lot)	118.0[e]
Carbon steel	Kure Beach (250-m lot)	171.0[f]
		142.1[g]
		81.8[h]
Carbon steel	Kure Beach (250-m lot)	71.9[i]
Carbon steel	Point Reyes, California	76.8[j]
Carbon steel	Kure Beach (200-m lot)	20.7[k]

Note: (a) Based on Kucera and Mattson (1982); (b) Based on Southwell and Bultman (1975); (c) Based on Knotkova et al. (2012); (d) Based on Morcillo et al. (1995); (e) Based on Copson (1960); (f) Reference 9 in Albrecht and Hall, Jr. (2003); (g) Reference 11 in Albrecht and Hall, Jr. (2003); (h) Reference 12 in Albrecht and Hall, Jr. (2003); (i) Based on ASTM Committee B-3 (1959); (j) Based on Melchers (2007); (k) Based on FHWA (2011).

Table 2.2 Corrosion rate data of stainless steel plates

Environment	Steel Type	Corrosion Rate	Corrosion Rate Ratio
Rural	Mild steel	22μm/year[a]	-
	AISI 410	0.03μm/year[a]	1.36×10^{-3}[a]
Urban	Mild steel	53μm/year[a]	-
	AISI 410	0.04μm/year[a]	7.55×10^{-4}[a]
Marine	Mild steel	36μm/year[a]	-
	AISI 410	0.04μm/year[a]	$\mathbf{1.11\times 10^{-3}}$[a]
Marine (Kure Beach 250-m lot)	Mild steel	23.69μm/year[b]	-
	11.6% Cr steel	0.64μm/year[b]	**0.027**[b]
	12.2% Cr steel	0.32μm/year[b]	**0.0135**[b]
Marine (Kure Beach 200-m lot)	Carbon steel	20.7μm/year[c]	-
	A709-50CR	1.10μm/year[c]	0.0534[c]

Note: (a) Based on Kucera and Mattson (1982); (b) Based on Knotkova et al. (2012) and Schmitt and Mullen (1968); (c) Based on FHWA (2011). The data used to fit a distribution appear in bold.

Corrosion Model

Corrosion of steel bridge girders can be attributed to the deicing salt running off the deck, salt due to traffic below the bridge, and/or airborne salt from nearby coastline. In this report, it is assumed that the corrosion rate in all three scenarios is similar to that obtained from atmospheric exposure tests in mild marine environments. The thickness loss of steel plates under atmospheric corrosion can be modeled using the equation (Albrecht & Naeemi, 1984):

$$\Delta d(t) = A(t - t_0)^B \tag{2.1}$$

where t is the time of bridge in service (years), $\Delta d(t)$ is the thickness loss up to time t, t_0 is the coating life (years), and A and B are the coefficients obtained via fitting the time-variant corrosion loss data. The coefficient B reflects the rust detachment rate: $B = 0.5$ represents a case without any rust detachment, and further corrosion is controlled by diffusion of moisture and other substances; B larger than 0.5 indicates an accelerated diffusion process due to the rust detachment from the steel surface; B close to 1 indicates highly permeable rust and/or rapid rust detachment (Díaz et al., 2012).

For carbon steel, existing test results found that the mean of B can reach 0.79, with a standard deviation of 0.387 (Albrecht & Naeemi, 1984). This indicates a fast diffusion process and rapid rust detachment. Herein, $B = 1$ is used due to the lack of experimental data and the ease of model fitting. In this case, the coefficient A becomes the annual corrosion rate. The time-variant corrosion loss data in long-term exposure tests are analyzed to determine the value of this annual corrosion rate and its uncertainty. It should be noted that the corrosion of carbon steel develops extremely fast in a short, aerobic phase at the very beginning; the annual corrosion rate then stabilizes to a lower, constant value with the onset of an anaerobic phase (Melchers, 2007). The transition from aerobic to anaerobic phases often occurs after the first year of exposure and can be as long as 6 to 7 years. Corrosion rates obtained before this transition can severely overestimate the long-term corrosion loss. Therefore, the corrosion loss data shorter than 1 year should be excluded during the estimation of corrosion rates.

Despite the superior corrosion resistance of A709-50CR, it might still corrode, albeit extremely slowly, due to the breakdown of the passive layer at localized areas with high chloride concentration (Groshek, 2017). As mentioned previously, it is assumed herein that B in Eq. (2.1) is equal to 1 for A709-50CR. As the corrosion rate of A709-50CR is extremely small, the error introduced by this assumption should be negligible. In addition, A709-50CR does not require coating. Hence, the coating life t_0 is 0 in Eq. (2.1). Existing corrosion rate data of A709-50CR and similar types of stainless steel contain considerable uncertainty. This is because the breakdown of the passive layer, the mechanism responsible for A709-50CR corrosion, depends on various environmental parameters such as the concentration of the aggressive anions and the temperature. Therefore, rather than gather corrosion rate data directly, the ratio of the corrosion rate of A709-50CR to that of carbon steel exposed in the same environment is calculated based on existing test results. This corrosion rate ratio as well as its uncertainty is used to reflect the corrosion resistance of A709-50CR. Since test data on A709-50CR are scarce, the test results of martensitic stainless steel with a similar chromium content are also collected to determine the corrosion rate ratio. The collected test results are shown in Table 2.2.

Corrosion of Steel Rebars

Apart from steel girders, steel rebars in the concrete deck are also subject to chloride-induced corrosion. Corrosion can reduce the cross-sectional area of steel rebars, decreasing the structural capacity of the deck. When the composite action between the deck and the steel girders is considered (as in the case of composite steel bridges), corrosion of steel rebars can also lead to the decrease of the girder capacities. Chloride-induced corrosion of steel rebars initiates when the chloride concentration at the depth of a rebar reaches a critical value (Thoft-Christensen et al., 1996). This corrosion initiation time can be calculated based on Fick's second law, shown as follows (Enright & Frangopol, 1998):

$$T_i = \frac{X^2}{4D_c}\left[erf^{-1}\left(\frac{C_0 - C_{cr}}{C_0}\right)\right]^{-2} \quad (2.2)$$

where X is the concrete cover (mm), D_c is the chloride diffusion coefficient (mm^2/year), C_0 is the surface chloride concentration (kg/m^3), and C_{cr} is the critical chloride concentration at which corrosion starts (kg/m^3).

Chloride-induced corrosion of steel rebars usually takes the form of pitting corrosion (Gouda et al., 1975). The maximum pit depth along the rebar length direction can be expressed as (Val & Melchers, 1997):

$$p(t) = 0.0116 \cdot i_{corr} \cdot R \cdot (t - T_i) \quad (2.3)$$

where $p(t)$ is the maximum pit depth (mm), i_{corr} is the corrosion current density (μA/cm^2), t is the time in service (years), and R is the ratio of maximum pit depth over the penetration calculated based on uniform corrosion model. The shape of the pit and the remaining area of a corroded rebar can be determined based on Val and Melchers (1997).

REPAINTING INTERVAL OF CARBON STEEL GIRDERS

Due to potential corrosion damage, carbon steel bridges need repetitive repainting actions during their lifecycle. These actions are seen as an important difference, outside of initial cost, between A709-50CR and carbon steel bridges. It is decided that data from the National Bridge Inventory (NBI) (FHWA, 1992) should be used to support any time-interval assumptions made moving forward. The Federal Highway Administration supplies annual bridge inspection data through the NBI database. Each bridge within NBI is rated on a conditional rating scale from 0 to 9 for each of its three structural components: deck, superstructure, and substructure. A description of each of the ratings is shown in Table 2.3, with 9 being the highest rating and 0 being the lowest, in terms of bridge condition.

Table 2.3 National Bridge Inventory conditional rating scale

Condition Rating	Description
9	Excellent condition.
8	Very good condition: no problems noted.
7	Good condition: some minor problems.
6	Satisfactory condition: structural elements show minor deterioration.
5	Fair condition: all primary structural elements are sound but may have minor corrosion, cracking or chipping.
4	Poor condition: advanced corrosion, deterioration, cracking, or chipping.
3	Serious condition: corrosion, deterioration, or cracking and chipping have seriously affected superstructure; local failures are possible.
2	Critical condition: advanced deterioration of superstructure; may have cracks in steel or concrete; it may be necessary to close the bridge until corrective action is taken.
1	"Imminent" failure condition: major deterioration or corrosion in superstructure; bridge is closed to traffic but corrective action may put back in light service.
0	Failed condition: out of service; beyond corrective action.

Note: Based on FHWA (1992).

While the NBI database provides data for all bridges in the United States, using these data would be difficult and inappropriate without classifying each bridge according to atmospheric, marine, and de-icing salt exposure. Therefore, only steel girder superstructures in Pennsylvania are considered. Since Pennsylvania is within one climatically consistent region (Karl & Koss, 1984), all bridges can be grouped into the same level of exposure. Resultingly, any use of the data collected through this method should be applied only to bridges in similar levels of exposure and of the similar steel girder design.

As the coating on the steel girders degrades and the bridge begins to show signs of corrosion, the conditional rating is expected to decrease. Similarly, when the steel girders receive a repainting action, the expectation is that the conditional rating will increase. However, besides repainting, many other maintenance actions can also raise the condition rating. Therefore, it is difficult to infer the repainting interval directly from the NBI data. Instead, the repainting interval is herein represented by the coating life, which is relatively easier to infer from the data. Specifically, the coating life can be represented as the duration within which the superstructure conditional rating stays within a certain range of values. The repainting interval thus inferred is generally safe against inconsistencies in inspector's judgement from year to year as well as from the different types of maintenance actions. Using the descriptions of each conditional rating, as shown in Table 2.3, the best range of ratings to represent coating life would be between 8 and 5. This is the duration in which a superstructure starting at an "excellent" or "very good" condition begins to show "minor corrosion" (i.e., the coating is considered to have failed). An example of the identified coating life (used to represent repainting interval) is shown in Figure 2.1. It is possible to apply this definition to all steel superstructures that have consistent bridge data between 1992 and 2018 in the NBI database.

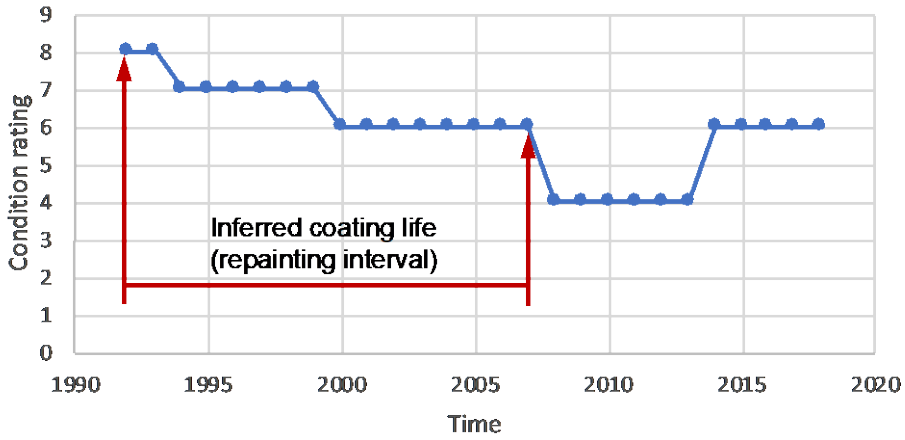

Figure 2.1 Example of inferred coating life (repainting interval)

Based on the aforementioned method, data of the coating life are shown in Figure 2.2 based on 128 steel bridges in Pennsylvania with complete information (i.e., ratings start from 8 or higher and drop to 5). The data are fitted to normal and lognormal distributions, as shown in Figure 2.2. The Anderson-Darling (AD) test was conducted and indicates that the coating life is best modeled as a lognormal distribution with a mean of 15.4 years and a standard deviation of 5.3 years.

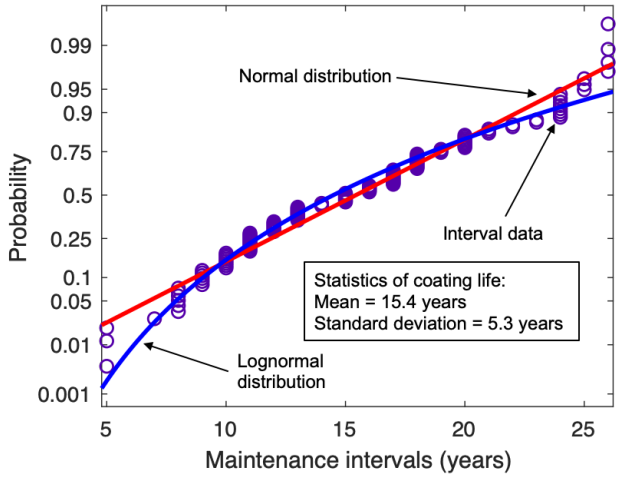

Figure 2.2 Data of inferred coating life (repainting intervals)

CHAPTER 3

Lifecycle Assessment

LIFECYCLE COST ASSESSMENT

Lifecycle cost of A709-50CR bridges has been investigated in several studies. Okasha et al. (2012) conducted a lifecycle cost analysis for A709-50CR and carbon steel girders. Three cost components were considered in their study: (1) material cost, (2) miscellaneous costs, and (3) repainting cost. The material cost includes the cost of A709-50CR or conventional carbon steel. Miscellaneous costs include those from fabrication, initial painting, shop inspection, and transportation cost. The repainting cost is only present for carbon steel girders. It was found that although an A709-50CR girder is 33.6% more expensive than a carbon steel girder of the same dimensions, the lifecycle cost of the A709-50CR girder is significantly lower due to the avoidance of repetitive repaintings.

Based on Okasha et al.'s (2012) initial study, Soliman and Frangopol (2015) performed a lifecycle cost analysis for A709-50CR and carbon steel girders using an improved lifecycle cost model. Both direct and indirect costs associated with a repainting action were considered. The direct cost is based on Okasha et al.'s (2012) data, while the indirect cost includes economic losses due to repainting-related detour and environment costs. It was again demonstrated that the total lifecycle cost of an A709-50CR girder can be much lower than that of a carbon steel girder of the same dimensions.\

Although the lifecycle cost of A709-50CR bridges has been investigated thoroughly in the aforementioned studies, there is a lack of comprehensive studies on the lifecycle environmental impacts of A1010 steel bridges. For instance, Soliman and Frangopol's (2015) study only considered the carbon dioxide (CO_2) emissions. Therefore, this chapter aims to fill in this gap in the understanding of the lifecycle performance of A709-50CR bridges.

LIFECYCLE ENVIRONMENTAL ASSESSMENT

Assessment Framework

Lifecycle environmental assessment (LCEA, also known as lifecycle environmental analysis or cradle-to-grave environmental analysis) is a technique to assess environmental impacts associated with all the stages within a product's lifespan from raw material extraction to material processing, manufacturing, operation, maintenance, and disposal or recycling. The main goal of LCEA is to "compare the full range of environmental effects assignable to products and services by quantifying all inputs and outputs of material flows and assessing how these material flows affect the environment" (Turconi et al., 2013). The results of LCEA can be used to: (i) improve the process of production; (ii) help decision makers choose better products, and (iii) support the related policy to protect our environment.

The main purpose of LCEA in this study is to help decision makers to choose between A709-50CR and conventional carbon steel for bridge construction. As mentioned in Chapter 2, A709-50CR contains heavy metal elements such as chromium, manganese, and nickel, which may cause significant CO_2 emissions and other environmental impacts (e.g., severe pollution to soil and water) during the mining process. In addition, A709-50CR steel requires special fabrication processes such as plasma cutting and welding, which can have detrimental environment impacts. However, akin to lifecycle cost analysis, the superior corrosion resistance of A709-50CR indicates less environmental impacts during the service life. Hence, an LCEA is needed to quantify the advantages/disadvantages of A709-50CR bridges.

ISO 14040 (2006) and ISO 14044 (2006) are two international standards for LCEA. According to ISO 14040 (2006), LCEA comprises two major stages:

(a) Compiling an inventory of relevant inputs and outputs (lifecycle inventory analysis);
(b) Evaluating the potential environmental impacts associated with the inventory (lifecycle impact analysis).

Lifecycle inventory (LCI) analysis uses the input-output method to create an inventory flow associated with the product under consideration. The input usually includes raw materials and energy, while the output includes emissions to air, water, and soil. The inventory flow should contain all activities in the production chain and give a clear picture of the technical system boundaries.

LCI analysis is followed by lifecycle impact assessment (LCIA). LCIA groups relevant inventory results to evaluate potential environmental damage in different aspects such as global warming potential, acidification potential, and eutrophication potential, among others. For example, the global warming potential can be determined based on LCI results of CO_2 and other greenhouse gas (GHG) emissions.

Lifecycle Inventory Analysis

For LCI analysis, the product category rules should be first specified. These rules set out technical details of LCI analysis including functional/declared unit, reference service life, boundary settings, recycling declaration, and the system of measurement. In this chapter, the declared unit for environmental impacts is defined as one year; that is, the lifecycle inventory and impact results are calculated annually. For application to bridges, the design service life of a bridge (i.e., 75 years) is used as the reference service life (RSL). For reporting results, the International System of Units (SI units) are used for inventory and impact analyses. Overall, three types of inorganic gases emissions are investigated, including carbon dioxide (CO_2), sulfur dioxide (SO_2), and nitrogen oxides (NO_x).

The system boundary is adapted from the report by the Swedish Transport Administration (2016). In particular, the RSL is divided into three stages: (i) initial stage, (ii) maintenance stage, and (iii) demolition and recycling stage. A summary of different emissions considered is listed in Table 3.1.

Table 3.1 Stages of lifecycle inventory analyses

Stage	Emissions Considered
Initial	Steel production (including mining, furnacing, and other processes of steel production)
	Initial painting (for carbon steel girders only)
Maintenance	Direct emissions of repainting (including the embedded emissions of repainting materials)
	Indirect emissions associated with repainting (due to exhaust of on-detour vehicles)
Demolition & Recycling	Recycled steel scraps (this will be considered separately in the initial stage)

Note: Emissions deemed the same for both A709-50CR and carbon steel girders are not considered.

The initial stage consists of emissions caused by raw material acquisition, steel production, and bridge construction. The only difference in the initial stage is assumed to arise from material-related emissions. Other emissions such as those from transportation, machinery, and construction are not included, since they tend to be the same for both steel materials. According to personal communication with ArcelorMittal, the emissions caused by cutting and welding of A709-50CR, though slightly higher, can be considered the same as those associated with carbon steel. Hence, these emissions are neglected in this study.

The maintenance stage includes direction emissions due to maintenance actions and the associated indirect emissions due to detour and congestion. In this study, only repainting is considered during the maintenance stage of carbon steel bridges. Other types of maintenance actions such as patching are neglected, since they are expected to be the same for A709-50CR and carbon steel bridges. In addition, based on the corrosion data presented in Chapter 2, A709-50CR girders do not need any repainting.

During the demolition and recycling stage, the demolition-related emissions are similar for both A709-50CR and carbon steel. Hence, the demolition emissions are not taken into account. It is noted that part of the steel in a demolished girder can be recycled. The recycled steel scraps can reduce the initial emissions of both A709-50CR and carbon steel. Nonetheless, the benefit of using steel scraps in A709-50CR production is less salient due to the need of other heavy metals.

Lifecycle Impact Assessment

As mentioned previously, lifecycle impact assessment (LCIA) aims to connect LCI results to the corresponding environmental impacts categories. According to ISO 14040 (2006), each impact category can be represented by an impact indicator, which is then related to one or multiple LCI results. For example, the greenhouse gas emissions (e.g., CO_2 and CH_4 emissions) can be connected to the global warming potential, an impact category, using the impact indicator of CO_2 equivalent emissions (termed herein as CO_2-eq). The conversion system IMPACT 2002+, first proposed by Jolliet et al. (2003), is adapted to bridge LCIA in this study. Table 3.2 presents the relation between inventory results and impact categories.

Table 3.2 Conversion from inventory to impact results

Impact Category	Related Inventory	Indicator
Global warming potential (GWP)	CO_2	CO_2-eq
Acidification potential (AP)	SO_2 and NO_x	SO_2-eq, or NO_x-eq
Eutrophication potential (EP)	NO_x	N-eq

Note: Based on Jolliet et al. (2003).

For global warming potential, CO_2 emissions are the only relevant inventory result considered in this study. The conversion to CO_2-eq is straightforward; namely, one unit weight of CO_2 emissions is equivalent to one unit weight of CO_2-eq. Acidification is a process in which pH falls in aquatic ecosystems as a result of SO_2 and NO_x depositions. Acidification potential can be represented by either SO_2- or NO_x-equivalent (SO_2-eq or NO_x-eq). In this study, acidification potential is measured by SO_2-eq. The conversion factor from NO_x to SO_2-eq is 0.7 (GHK/BioIS, 2006); that is, one unit weight of NO_x emissions is equivalent to 0.7 unit weight of SO_2-eq. Finally, eutrophication is the process caused by nitrogen and phosphate elements in water (Kim & Chae, 2016). It is extremely harmful for aquatic ecosystems. In this study, eutrophication potential is measured by nitrogen-equivalent (N-eq). One unit weight of NO_x emissions can be converted to 0.48 unit weight of N-eq (Heijungs, 1992).

LCEA OF A709-50CR AND CARBON STEEL GIRDERS

Inventory Data in the Initial Stage

Inventory results in the initial stage can be obtained by considering each inventory category by girder weight. In addition, the emissions associated with the initial painting should be included for carbon steel girders. The inventory data used in this stage are introduced in this subsection.

Metal production processes for A709-50CR and carbon steel are summarized in Table 3.3 (Norgate et al., 2007). There are two main types of steel production: (a) basic oxygen furnace (BOF), in which steel is produced by blowing oxygen through heated pig iron; and (b) electric arc furnace (EAF), in which steel, usually recycled scrap, is melted down to a liquid phase and then reformed. These two processes have different rates of emissions that are summarized in Table 3.4 for A709-50CR and carbon steel, respectively. Through communication with ArcelorMittal (personal communication 2019), it is considered that about 33% of all steel production in the United States uses BOF, while the other 67% uses EAF. In addition to steel production, emissions relating to feedstock acquisition are also considered, as presented in Table 3.5. As a type of stainless steel, A709-50CR needs argon oxygen decarburization (AOD) to reduce carbon content. This process may produce higher CO_2 emissions for A709-50CR (Norgate et al., 2007).

Table 3.3 Metal production processes

Metal	Feedstock	Process
Carbon steel	Iron ore (64% Fe)	Integrated route: blast furnace (BF) and basic oxygen furnace (BOF) or electric arc furnace (EAF)
A709-50CR	Pig iron (94% Fe) Chromite ore (27.0% Cr, 17.4% Fe) Laterite ore (2.4% Ni, 13.4% Fe)	Electric arc furnace (EAF) and argon-oxygen decarburization (AOD)
Zinc (for painting)	Sulfide ore (5.5% Pb, 8.6% Zn)	Electrolytic process

Note: Based on Norgate et al. (2007); percentage values are in weight.

Table 3.4 Emission rates for producing A709-50CR and carbon steel

Emissions	A709-50CR Production	Carbon Steel Production
CO_2 (ton/ton production)	0.98 to 1.4[a]	1.6 to 2.2 for BOF[c] 1.4 to 2.0 for EAF[c]
SO_2 (kg/ton production)	0.16 to 0.18[b]	0.091[b]
NO_x (kg/ton production)	0.12 to 0.14[b]	0.011[b]

Note: (a) ISSF (2019) and Norgate et al. (2007); (b) (U.S. Environmental Protection Agency (2006) (2006); (c) International Energy Agency (2019).

Table 3.5 Emission rates associated with feed stock acquisition

Emissions	Iron	Nickel	Chromium (from ferrochrome)	Zinc
CO_2 (ton/ton acquisition)	0.20	11.1	5.1	4.6
SO_2 (kg/ton acquisition)	7.0	44.6	29.6	42.0
NO_x (kg/ton acquisition)	12.6	107.0	18.0	18.0

Note: Based on Norgate et al. (2007).

Combining the emissions in feedstock acquisition and production phases, the total initial emission rates of A709-50CR and carbon steel can be computed. They are summarized in Table 3.6. Due to the lack of data, initial emissions are assumed to follow triangular distributions. The mean value is computed as the average value of the upper and lower bounds. To calculate the emissions associated with the initial painting, it is assumed that zinc-epoxy primer (Valspar Industrial Mix, 2016) is used. The density of this primer is 3.03 kg/m^3, in which 85% by weight is zinc. The primer used in the initial painting is determined by the surface area of a girder and a dry firm thickness of 50 to 100 μm (again, triangular distribution is assumed for this thickness).

Table 3.6 Total emission rates of A709-50CR and carbon steel

Emissions	A709-50CR	Carbon Steel	Zinc (for initial painting)
CO_2 (ton/ton production)	3.4 to 3.9	1.5 to 2.1	4.6
SO_2 (kg/ton production)	20.0 to 22.0	7.2	42.0
NO_x (kg/ton production)	24.9 to 44.1	12.7	18.0

Note: Total emissions rates include emissions from production and acquisition phases; data without ranges are considered to be deterministic values.

Emissions in the Maintenance Stage

Carbon steel girders need several repainting actions over the course of their service life. These actions have detrimental environmental impacts that can be divided into two parts: the emissions caused by repainting actions themselves (direct emissions) and the emissions caused by repainting-induced detour (indirect emissions). In this study, the emissions caused by repainting the steel are considered to be the same as those associated with the initial painting.

The indirect emissions caused by detour can be estimated as (Gallivan et al., 2010):

$$E_d = \left[E_{d,c} \cdot (1 - T) + E_{d,t} \cdot T\right] \cdot d \cdot ADT \cdot l \cdot \rho_S \tag{3.1}$$

where $E_{d,c}$ and $E_{d,t}$ are the emissions (CO_2, SO_2, or NO_x) per kilometer traveled by on-detour cars and trucks (kg CO_2/km), respectively; ρ_S is the ratio of emissions from vehicles traveling at the restricted speed to those from vehicles traveling at the unrestricted speed; d is the duration of detour; l is the detour length; T is the proportion of truck traffic in average daily traffic (ADT). Due to the lack of reliable data, it is assumed herein that ρ_S is the same for both types of vehicles and for all types of emissions considered. The variables in Eq. (3.1) are summarized in Table 3.7. For a specific bridge, T, ADT, and l can be found from the National Bridge Inventory (FHWA, 1992).

Table 3.7 Variables for emissions calculation in the maintenance stage

Random Variable	Description	Unit	Distribution[a]
$Ecn_{d,c}$	Emissions per kilometer for cars	kg CO_2/km	LN(0.22, 0.2)[b]
		mg SO_2/km	TR(0.08, 0.11, 0.14)[c]
		mg NO_x/km	TR(0.71, 0.73, 0.75)[c]
$Ecn_{d,t}$	Emissions per kilometer for trucks	kg CO_2/km	LN(0.56, 0.2)[b]
		mg SO_2/km	TR(2.24, 2.73, 3.22)[c]
		mg NO_x/km	TR(3.36, 3.82, 4.28)[c]
ρ_S	Emission ratio at different speeds	-	1.40[b]
D	Duration of detour	days	15[d]

Note: (a) LN = Lognormal distribution (the two parameters are the mean and the standard deviation, respectively); TR = Triangular distribution (the three parameters are the lower bound, the mode, and the upper bound, respectively); Deterministic variables are directly represented by their corresponding values; (b) Based on Gallivan et al. (2010); (c) Based on Kirchstetter et al. (1999); (d) Assumed.

Consideration for the Recycling Stage

After the demolition of a bridge, about 90% of the generated steel scrap can be recycled (Gervásio et al., 2015). The recycled steel scrap can be remelted in the furnace and thus substitute pig iron as raw material.

Hence, the emissions associated with raw material acquisition can be reduced for both A709-50CR and carbon steel. However, despite recycled steel scrap, A709-50CR still needs other raw materials such as chromium. Since A709-50CR scrap is magnetic, it is hard to be recycled separately after being mixed with conventional carbon steel in the demolition process. Therefore, A709-50CR production still needs acquisition of chromium. To consider the benefit of recycling, the reduction in CO_2 emissions is considered for both A709-50CR and carbon steel in the initial stage. However, SO_2 and NO_x emissions cannot be effectively reduced by using recycled steel scraps, as they are related to the use of chromium. Table 3.8 lists the total CO_2 emission rates in steel production with and without recycled steel scrap.

Table 3.8 Total emission rates with recycled steel scrap

Emissions	A709-50CR	Carbon Steel
CO_2 (ton/ton production)	1.5 to 2.0	0.1 to 0.6
SO_2 (kg/ton production)	13.5 to 15.5	0.2
NO_x (kg/ton production)	12.7 to 31.9	0.1

Note: Based on Norgate et al. (2004); total emissions rates include emissions from production and acquisition phases; data without ranges are considered to be deterministic values.

Preliminary LCEA Results of A709-50CR and Carbon Steel Girders

Based on the data presented in the previous subsection, a preliminary LCEA was conducted based on a steel girder bridge, adapted from the E-17-AH bridge in Colorado (Estes & Frangopol, 1999). This bridge has three simply supported spans of equal length (13.3 m) and a total length of 42.1 m. The bridge has two exterior (WF 33×132) girders and seven interior (WF 33×125) girders. The cross sections are shown in Figure 3.1. The total weight of all nine steel girders is 69.75 metric tons, while the total surface area for painting is 1,043.45 m^2. It is assumed that the nine girders can be made of either carbon steel or A709-50CR. The time horizon under consideration is 75 years, in which repainting actions are implemented based on the time interval presented in Chapter 2 (i.e., it follows lognormal distribution with the mean of 15.4 years and the standard deviation of 5.3 years). To take into account the uncertainties, Monte Carlo simulation with 100,000 samples are used to calculate the lifecycle inventory and impact values.

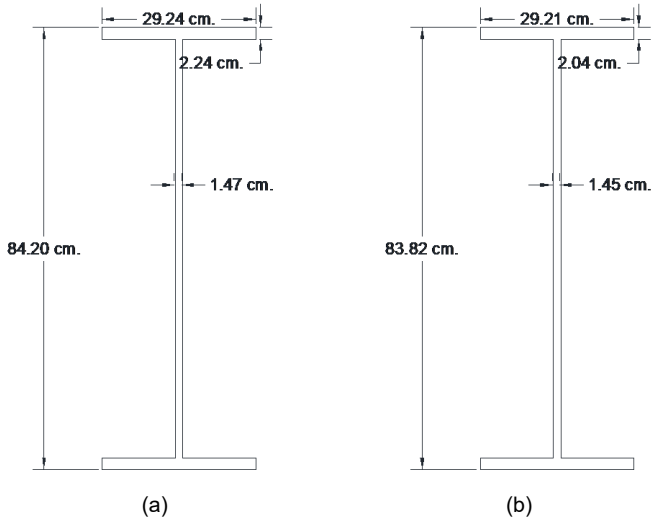

Figure 3.1 Steel girder dimensions: (a) exterior girders and (b) interior girders

The LCI results are presented in Figure 3.2 for different cases under consideration. The results show that the initial CO_2 and NO_x emissions associated with carbon steel girders are lower than those associated with

A709-50CR girders. However, the lifecycle CO_2 and NO_x emissions associated with carbon steel girders will exceed those associated with A709-50CR girders. The mean breakeven time occurs after around 15 years in service. Both the initial and the lifecycle SO_2 emissions associated with A709-50CR girders are higher than those associated with carbon steel girders. The reason is that the nickel ore extraction can emit a large amount of SO_2. This observation highlights the need to use recycled nickel in A709-50CR production.

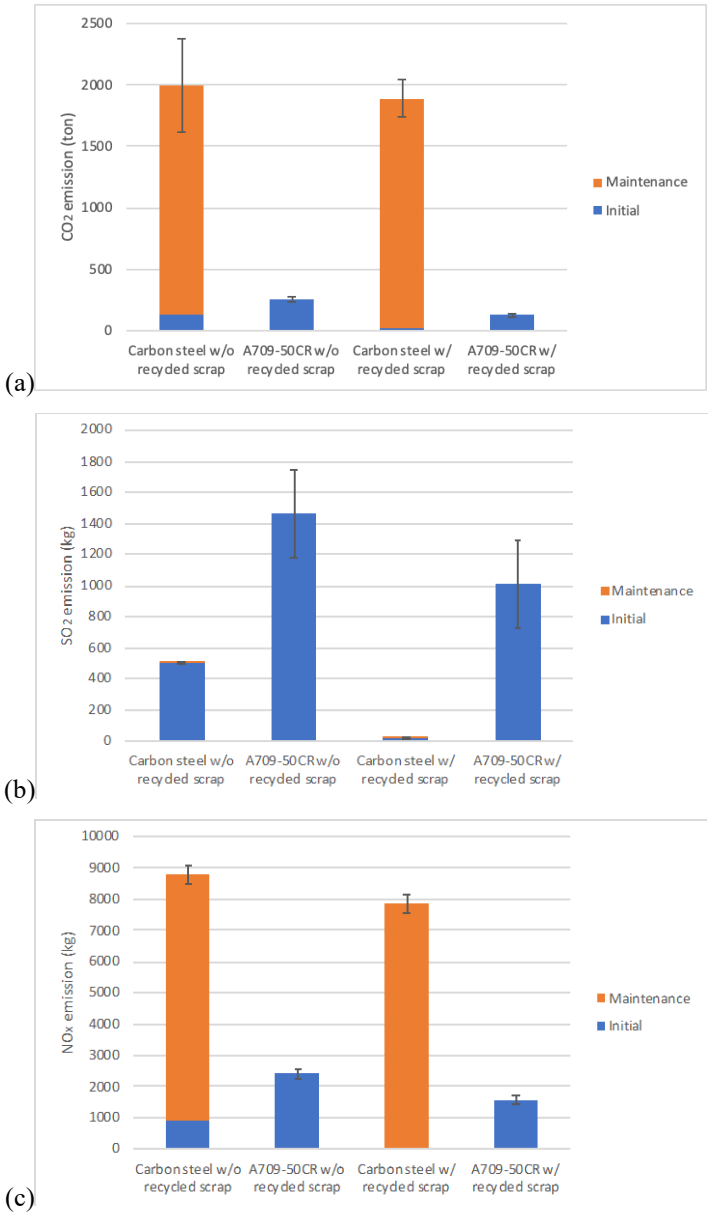

Figure 3.2 Results of lifecycle inventory analysis (error bar indicates mean ± standard deviation): (a) CO_2 emission, (b) SO_2 emission, and (c) NO_x emission

Based on the conversion methods introduced in the previous subsection, the results of LCIA are shown in Figure 3.3. The results of LCIA show that the initial global warming potential (GWP), acidification potential (AP), and eutrophication potential (EP) values associated with carbon steel girders are lower than those associated with A709-50CR girders. However, the lifecycle GWP, AP, and EP values associated with

carbon steel girders are significantly higher than those associated with A709-50CR girders. For GWP and EP values, the breakeven time occurs after around 15 years in service, while for AP value it will take on average 30 years in service until A709-50CR girders become more advantageous than carbon steel girders.

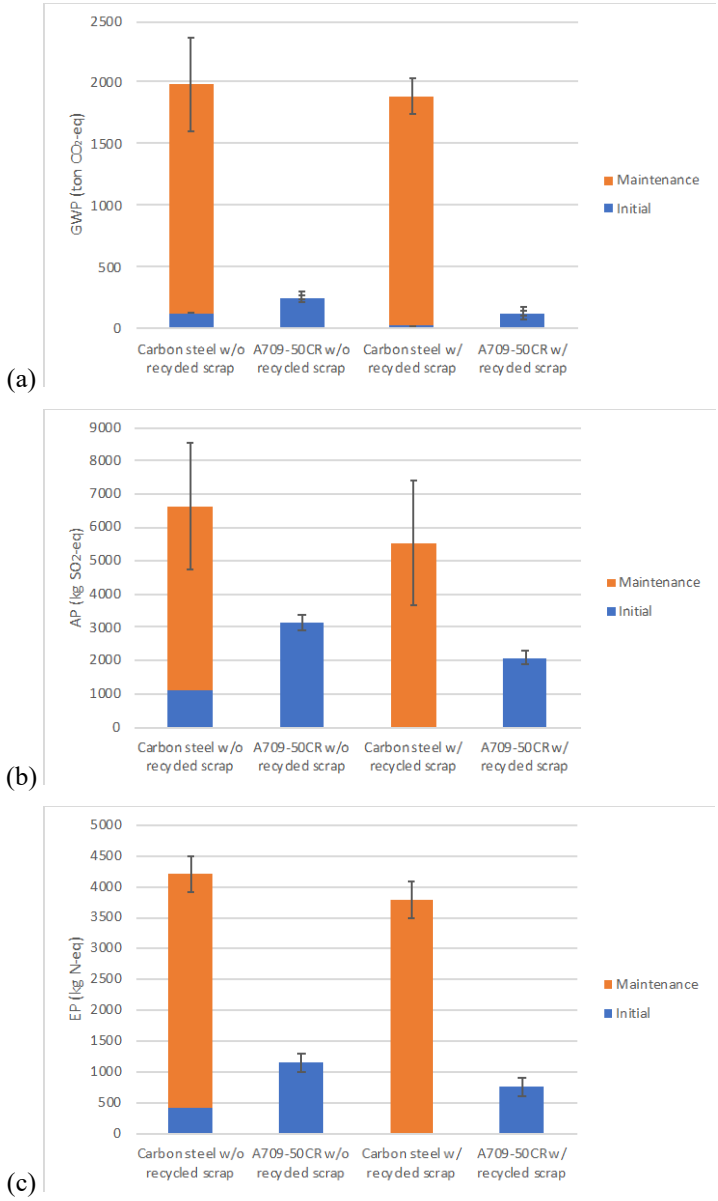

Figure 3.3 Results of lifecycle impact assessment (error bar indicates mean ± \standard deviation): (a) global warming potential (GWP), (b) acidification potential (AP), and (c) eutrophication potential (EP)

CHAPTER 4

Risk-based Lifecycle Optimization

A709-50CR FOR BRIDGE MAINTENANCE

Based on the existing lifecycle cost analysis and the lifecycle environmental assessment in the previous chapter, A709-50CR girder bridges exhibit considerable economic, social, and environmental benefits due to the avoidance of repetitive maintenance actions. However, the possibility of using A709-50CR in maintenance actions of existing steel bridges is yet to be fully explored. To achieve cost effectiveness of bridge rehabilitation, maintenance actions are usually determined based on lifecycle reliability/risk analysis (Akgül, 2002; Barone & Frangopol, 2014a, 2014b; Estes, 1997). However, most existing lifecycle maintenance frameworks deal with maintenance actions using the original deterioration-susceptible materials. Incorporation of durability-enhancing materials such as A709-50CR can pose additional modeling and computational challenges (Yang et al., 2019). This chapter presents methodologies to investigate the use of A709-50CR in girder replacement actions. It is proposed that besides new constructions, A709-50CR girders can also be used to replace corroded carbon steel girders in aging multi-girder steel bridges. Specifically, for bridge superstructures made up of only carbon steel girders and those made up of both types of steels, system reliability analysis is introduced herein to obtain time-variant reliability profiles. Based on the reliability profiles and the associated failure risk, lifecycle optimization can be conducted to determine when and which girders have to be replaced.

RISK ASSESSMENT OF STEEL GIRDER BRIDGES

Performance Function of Girder Bridges

To conduct reliability analysis, a generalized performance function can be expressed as

$$g = R(\boldsymbol{x}_R) - S(\boldsymbol{x}_S) \tag{4.1}$$

where g is the safety margin; R and S are the load-carrying capacity (also called structural capacity) and the load effect associated with a failure mode, respectively; and $\boldsymbol{x}_R$ and $\boldsymbol{x}_S$ are the vectors of random variables associated with R and S, respectively. The safety of girders is prioritized in this study, since their failure consequences are much larger than that of bridge decks. For each girder, two failure modes are considered: flexural failure and shear failure. Strength I load combination (AASHTO, 2017) relating to normal vehicular use on the bridge is considered to estimate load effects, as it usually controls the design of superstructure of small- to medium-span girder bridges.

Structural analysis is carried out prior to reliability analysis to determine the load effects from dead and live loads. The dead load of a bridge superstructure comprises the weight of concrete slabs, concrete barriers,

future wearing surfaces, steel girders, and attached appurtenances and utilities. The self-weight of steel girders is usually estimated by weight per square meter on the bridge deck.

The vehicular live load is determined based on AASHTO LRFD specifications (AASHTO, 2017). This load, designated as HL-93, includes a design lane load and a design truck or a design tandem (whichever generates larger live load effects in structural components) (AASHTO, 2017). The flexural capacity of a composite steel girder is reached when the entire section is in plastic domain. According to AASHTO (2017) Article 6.10.7.1.2, the flexural capacity of a composite section controlled by plastic deformation shall be calculated as

$$M_n = \begin{cases} M_p & \text{if } D_p \le 0.1D_t \\ M_p(1.07 - 0.7D_p/D_t) & \text{otherwise} \end{cases} \tag{4.2}$$

where D_p is the distance from the top of the concrete deck to the neutral axis of the composite section when it reaches full plasticity; D_t is the total depth of the composite section; and M_p is the plastic moment of the composite section, calculated using AASHTO (2017) Table D6.1-1 based on neutral axis positions.

The shear capacity of a composite girder depends on whether the web is sufficiently stiffened to avoid local buckling. Based on AASHTO (2017) Article 6.10.9, the shear capacity of an unstiffened composite girder is

$$V_{unstiff} = CV_p = C \cdot 0.58F_yDt_w \tag{4.3}$$

where V_P is the plastic shear load-carrying capacity; C is the ratio of the shear-buckling resistance to the shear yield strength; D and t_w are the height and thickness of the web, respectively; and F_y is the yield strength of the web. The ratio C is computed as follows:

$$C = \begin{cases} 1.0 & \text{if } \frac{D}{t_w} \le 1.12\sqrt{\frac{Ek}{F_y}} \\ \frac{1.12}{D_{tw}}\sqrt{\frac{Ek}{F_y}} & \text{if } 1.12\sqrt{\frac{Ek}{F_y}} < \frac{D}{t_w} \le 1.40\sqrt{\frac{Ek}{F_y}} \\ \frac{1.57}{(D_{tw})^2}\left(\frac{Ek}{F_y}\right) & \text{if } \frac{D}{t_w} > 1.40\sqrt{\frac{Ek}{F_y}} \end{cases} \tag{4.4}$$

where E is the elastic modulus of steel; k is the shear buckling coefficient expressed as $k = 5 + 5/(d_0/D)^2$. For a stiffened composite girder, the shear capacity can be computed as

$$V_{stiff} = \begin{cases} \left[C + \frac{0.87(1-C)}{\sqrt{1+\left(\frac{d_0}{D}\right)^2}}\right] \cdot V_p & \text{if } \frac{2Dt_w}{(b_{fc}t_{fc}+b_{ft}t_{ft})} \le 2.5 \\ \left[C + \frac{0.87(1-C)}{\sqrt{1+\left(\frac{d_0}{D}\right)^2}+\frac{d_0}{D}}\right] \cdot V_p & \text{otherwise} \end{cases} \tag{4.5}$$

where b_{fc} and t_{fc} are the width and thickness of the flange in compression, respectively; and b_{ft} and t_{ft} are the width and thickness of the flange in tension, respectively. Both the time-variant flexural and shear failure of composite girders are of a random nature due to the aleatory uncertainties such as material properties and geometry dimensions as well as the epistemic uncertainties due to model error of design

equations and deterioration models (Ang & Tang, 2007). The spatial corrosion pattern in which corrosion develops on the top surface of the bottom plate and the two sides of the web is adopted.

Correlation between load-carrying capacities of different girders is of great significance to reliability analysis. This correlation originates from the correlation of geometry sizes of members, material properties, and corrosion rates. It can also be due to the fabrication techniques, workmanship, and the spatial variability of environmental stressors. Herein, correlation is considered between flexural/shear capacities of different girders as well as flexural and shear capacities within one girder. Due to the lack of experimental evidence, a correlation coefficient equal to 0.9 is assumed for material strengths (i.e., steel yield strength and compressive strength of concrete) of different girders. The same correlation coefficient is assumed for corrosion rates of different girders. Within one girder, full correlation is considered for the material strength and corrosion rate. During the lifecycle of a bridge, the aforementioned correlation condition is used for flexural and shear capacities of girders replaced at the same time. Since maintenance actions usually span over several years, material strengths and corrosion rates are assumed to be independent among replaced and original girders as well as girders replaced at different times.

Reliability Analysis

A bridge is a structural system made up of multiple components. Therefore, it is necessary to estimate the probability of failure from a system perspective. Failure of a component can result in the failure of an entire system (series model), or systems may have redundancies where multiple components must fail before system failure (parallel model). It is worth noting that the component in reliability analysis refers to the individual failure modes. This term is different from the meaning of component in structural analysis.

For a girder bridge, the component reliability index β can reflect the safety associated with a specific failure mode (flexural or shear) of an individual girder. It can be determined using the first-order reliability method (FORM). The failure probability P_f is then calculated as

$$\mathrm{P_f} = \Phi(-\beta) \tag{4.6}$$

where $\Phi(\cdot)$ is the cumulative distribution function (CDF) of the standard normal distribution. Within FORM, the reliability index β is obtained by first locating a design point $\boldsymbol{u}^*$on the failure surface representing zero safety margin (i.e., $g = 0$ in Eq. (4.1)). This point marks the shortest distance of the failure surface to the origin in the reduced normal space. If the failure surface is approximated by a linear function at the design point, this shortest distance becomes the reliability index. In the reduced normal space, the direction vector pointing from the origin to the design point is termed as the alpha vector (Hohenbichler & Rackwitz, 1986). In a system made up of multiple components, the alpha vector of a component needs to be expanded to the reduced normal space at the system level (Hohenbichler & Rackwitz, 1986).

For simple series and parallel systems, their failure probabilities can be determined directly based on the results of component reliability analysis. According to Hohenbichler and Rackwitz (Hohenbichler & Rackwitz, 1983), the failure probability of a series system can be expressed as

$$\mathrm{P_{fsys}} = 1 - \int_{-\infty}^{\beta_1} \cdots \int_{-\infty}^{\beta_N} \frac{1}{\sqrt{(2\pi)^m |\boldsymbol{\Sigma}|}} \times \exp\left(-\frac{1}{2}\boldsymbol{\theta}^T \boldsymbol{\Sigma} \boldsymbol{\theta}\right) \mathrm{d}\boldsymbol{\theta} \tag{4.7}$$

and for parallel system

$$\mathrm{P_{fsys}} = \int_{\beta_1}^{\infty} \cdots \int_{\beta_N}^{\infty} \frac{1}{\sqrt{(2\pi)^m |\boldsymbol{\Sigma}|}} \times \exp\left(-\frac{1}{2}\boldsymbol{\theta}^{\mathrm{T}}\boldsymbol{\Sigma}\boldsymbol{\theta}\right) \mathrm{d}\boldsymbol{\theta} \tag{4.8}$$

where P_{fsys} is the system failure probability of a system; β_i $(i = 1,2,\dots,N)$ is the reliability index associated with failure mode i; $\boldsymbol{\theta} = \{\theta_1, \theta_2, \dots, \theta_N\}$ is the uncorrelated standard normal space where each dimension represents a failure mode; $\boldsymbol{\Sigma}$ is the correlation matrix of standard normal variates with diagonal elements equal to 1 and off-diagonal elements defined by ρ_{ij} (correlation coefficient between the ith and jth failure modes). The multi-dimensional integration can be calculated using the quasi Monte Carlo simulation method proposed by Genz (1992)

In system reliability calculation, the correlation can be attributed to correlated random variables or common random variables existing in multiple performance functions. For instance, the flexural/shear resistance of an interior girder can appear in different parallel-series subsystems. For a steel bridge, the load-carrying capacities of different girders also have correlation, as explained previously. Based on the linear approximation of the failure surface, the correlation coefficient ρ_{ij} can be approximated by $\alpha_i^T \alpha_j$, where α_i and α_j are the alpha vectors associated with the ith and jth performance functions, respectively (Ditlevsen, 1979).

In this study, failure of a girder is controlled by either flexural or shear failure, and thus modeled by a series model with two components. For a multi-girder bridge, excessive deflection causing the failure of bridges may only occur when several adjacent girders reach their ultimate limit states. Therefore, the system model for the multi-girder superstructure takes the form of several parallel-series subsystems connected with each other in series. Each subsystem consists of several adjacent girders. The system model is shown in Figure 4.1. Finite element (FE) analysis can be conducted to determine the number of adjacent girders.

For general systems that include both series and parallel subsystems, the equivalent component method (Gollwitzer & Rackwitz, 1983) can be used to calculate system reliability. In this method, the series-parallel system in Figure 4.1 is converted to a simple series system by using equivalent components to substitute parallel-series subsystems that represent adjacent girders. The equivalent component has the same failure probability as that of the subsystem and an equivalent direction vector. This direction vector, often termed as an equivalent alpha vector, can be calculated through numerical methods (Estes, 1997) or analytical solutions (Chun et al., 2015).

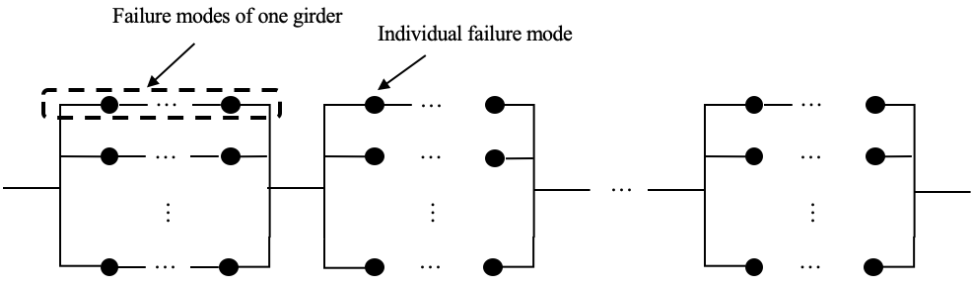

Figure 4.1 General system configuration for reliability analysis of bridge superstructure

Consequence Evaluation

Risk assessment combines the probability of an adverse event with the measurement of the consequences relating to the event (Ang & Tang, 1984). The risk associated with an event A, denoted herein as R_f, is defined as the product of the probability of event A (i.e., $P_f(A)$) and the consequence (i.e., C_A) associated with the event:

$$R_f = P_f(A) \cdot C_A \tag{4.9}$$

The lifecycle risk can be obtained by summing up the annual risk of each year during the service life. This method for calculating lifecycle risk is an approximation method that is valid in the cases of small annual failure probabilities.

Bridge failure results in direct cost to bridge owners, indirect consequences to the users of the transportation infrastructure and the local community, as well as environmental impacts due to bridge failure and reconstruction (Fiorillo & Ghosn, 2019). Direct costs usually include the demolition and rebuilding costs upon structural failure. Indirect social consequences entail the extra vehicle operating cost, congestion and delay cost, environmental cost, and cost of casualties in accidents (Fiorillo & Ghosn, 2019). The first two types are also known as the user cost. In this chapter, the direct cost is estimated by the rebuilding cost, and the user cost is used to represent indirect failure consequences. The environmental consequences can be estimated based on the results in Chapter 3. However, it is usually difficult to monetize the environmental impacts and use them in risk assessment (Z. Wang et al., 2019). One option to integrate economic, social, and environmental consequences in risk assessment is to apply multi-attribute utility theory (Sabatino et al., 2015). However, for brevity, only the economic and user consequences are considered in this chapter.

The rebuilding cost $C_{Reb}(t)$ is expressed as

$$\mathrm{C_{Reb}(t)} = \frac{\mathrm{c_{Reb} W L}}{(1+\mathrm{r})^{\mathrm{t}}} \tag{4.10}$$

where c_{Reb} is the rebuilding cost per square meter (USD/m^2); W and L are bridge width and length (m), respectively; and r is the discount rate of money. The extra vehicle operating cost $C_{Run}(t)$ is calculated as

$$\mathrm{C_{Run}(t)} = \left[\mathrm{c_{Run,car}}\left(1 - \frac{\mathrm{T_{ADT}}}{100}\right) + \mathrm{c_{Run,truck}}\frac{\mathrm{T_{ADT}}}{100}\right]\frac{\mathrm{D_l A_D d}}{(1+\mathrm{r})^{\mathrm{t}}} \tag{4.11}$$

where $c_{Run,car}$ and $c_{Run,truck}$ are the average costs for running cars and trucks per unit distance (USD/km), respectively; D_l is the net length of the detour (km); A_D is the average daily traffic (ADT); d is the duration of the detour (days); and T_{ADT} is the ratio of the average daily truck traffic (ADTT) to ADT (%). The time

needed to restore the bridge functionality (i.e., the duration of the detour) is assumed based on Decò and Frangopol (Decò & Frangopol, 2011): 36 months for ADT≤100; 24 months for 100<ADT≤500; 18 months for 500<ADT≤1,000; 12 months for 1,000<ADT≤5,000; and 6 months for ADT>5,000. Similarly, the congestion and delay cost $C_{TL}(t)$ is expressed as

$$C_{TL}(t) = \left[c_{AW} O_{Car}\left(1 - \frac{T_{ADT}}{100}\right) + (c_{ATC} O_{truck} + c_{goods})\frac{T_{ADT}}{100}\right]\frac{D_l A_D d}{S(1+r)^t} \quad (4.12)$$

where c_{AW} is the average wage per hour (USD/h); c_{ATC} is the average total compensation per hour (USD/h); c_{goods} is the time value of the goods transported in trucks (USD/h); O_{Car} and O_{Truck} are the average vehicle occupancies for cars and trucks, respectively; and S represents the average detour speed (km/h).

LIFECYCLE MAINTENANCE OPTIMIZATION

Using system reliability analysis and consequence evaluation, mentioned previously, the time-variant risk profile can be determined for a bridge superstructure. The maintenance action considered in this chapter is to replace the corroded carbon steel girders. Inevitably, maintenance actions can bring in additional lifecycle cost. Different intervention plans can render varied lifecycle risk and lifecycle maintenance costs. Therefore, intervention planning is an optimization problem to seek plans that can minimize both failure risk and maintenance cost. The lifecycle total maintenance cost can be expressed as:

$$C_{mx} = \sum_{i=1}^{N_{mx}} \frac{C_{rep,i}}{(1+r)^{t_i}} \quad (4.13)$$

where $C_{rep,i}$ $(i = 1 \dots N_{mx})$ is the repair cost of the ith maintenance action and t_i $(i = 1 \dots N_{mx})$ is the time of the ith maintenance action.

Similar to using carbon steel, replacing corroded carbon steel girders with A709-50CR can increase reliability and mitigate failure risk. In addition, the durability of the post-maintenance structure can be drastically enhanced. Therefore, using A709-50CR can possibly reduce the lifecycle maintenance cost while preserving the same or even larger safety margins. After this type of maintenance, bridges with both carbon steel and A709-50CR girders are referred to herein as hybrid bridges. The potential benefit of hybrid bridges in terms of lifecycle cost is investigated. It is worth noting that galvanic corrosion can occur when two metals with different electrochemical activity directly contact each other (Kucera & Mattsson, 1982). In this case, the more active metal may experience accelerated corrosion at and near the contact surface. This phenomenon can be a concern in hybrid bridges. To counter detrimental effect, local detailing measures such as adding sacrificing cover plate and/or inserting nonmetallic filling plates can be used.

In this chapter, a maintenance plan is described by the times of different girders to be replaced. To obtain optimal maintenance plans, the following bi-objective optimization is formulated:

Given

- The number of components considered for replacement M
- The maximum number of replacement actions for a girder N_r
- The corrosion model and the associated random variables H
- The maintenance cost and failure consequence C
- Service life of the structure T
- Monetary discount rate r

Find

- The replacement times of different girders $t_{mx} = \{t_1, t_2, t_3, \cdots, t_{M \cdot N_r}\}$

So that

- The expected lifecycle maintenance cost $E(C_{mx})$ and the lifecycle failure risk $E(C_f)$ are both minimized;

Subjected to

- The interval of two consecutive maintenance actions $\Delta t \geq 5.0$ years;
- The time of the first maintenance $t_1 \geq 10$ years;
- The time of the last maintenance $t_{M \cdot N_r} \leq T - 10$ years;
- $\beta_{min,annual} \geq \beta_{thr}$.where $\beta_{min,annual} = \{\beta_{min,1}, \beta_{min,2}, \ldots \beta_{min,N}\}$ is the vector containing the minimum annual reliability indices of the N failure modes of girders considered, and $\beta_{thr} = \{\beta_{thr,1}, \beta_{thr,2}, \ldots \beta_{thr,N}\}$ is the associated target reliability indices.

Nondominated Sorting Genetic Algorithm II (NSGA-II) (Deb et al., 2002) is adopted to carry out the optimization using the MATLAB global optimization toolbox (MathWorks, 2018). The obtained plans and their associated objectives are compared between carbon steel and A709-50CR maintenance actions. When the repair time of a certain girder (i.e., $t_i, i = 1 \ldots M \cdot N_r$) is out of the prescribed time range of maintenance actions (i.e., from 10 to $T - 10$ years), the girder does not need replacement.

CHAPTER 5

Case Study

CASE STUDY BRIDGE

The methods presented in Chapter 4 are illustrated in a case study. The goal of the study is to investigate the benefit of using A709-50CR for bridge maintenance (specifically, girder replacements). As mentioned previously, a large portion of bridges in Pennsylvania are steel bridges, among which over 80% (5,823 bridges) are classified as girder bridges. In this chapter, a four-girder bridge modeled based on a steel bridge located in Montgomery County, Pennsylvania, is studied to investigate the potential benefit of using A709-50CR for girder replacements. The bridge is a single-span, simply supported highway bridge carrying Cedar Hill Road and intersecting PA 309. The geometrical dimensions of the bridge are shown in Figure 5.1(a). The cross-section of the bridge superstructure and one of its girders are presented in Figure 5.1(b) and Figure 5.1(c), respectively. According to the bridge owner, the Montgomery bridge is a composite steel bridge. The two exterior girders are sufficiently stiffened transversely, while the webs of two interior girders are considered as unstiffened. Carbon steel (A709-50M) is used in both concrete reinforcement and steel girders.

STRUCTURAL CAPACITY

The flexural and shear capacities of the girders are computed based on AASHTO (2017), as presented previously. Corrosion is considered herein as the main cause of structural deterioration. The corrosion rate data inferred from existing corrosion test results are subject to distribution fitting and Anderson-Darling testing in order to obtain the most accurate probability distribution model to describe its uncertainty. Based on the data in Table 2.1, an exponential distribution with a mean of 0.067 mm/year (p-value = 0.92) is used to model the annual corrosion rate of carbon steel plates. Due to limited data for A709-50CR, a uniform distribution is assumed for the corrosion rate ratio between A709-50CR and carbon steel. The lower and upper bounds of this ratio are determined based on data in Table 2.2 for the marine atmospheric environment.

In order to infer the coating life and its uncertainty, superstructural condition rating data between 1992 and 2018 were collected for steel bridges in Pennsylvania. As stated previously, the coating life of a bridge is inferred from NBI data. The coating life thus obtained was modeled by a lognormal distribution with a mean of 15.3 years and a standard deviation of 5.3 years.

Full correlation is assumed between the pitting corrosion losses in different rebars. This assumption is acceptable, since the corrosion of steel rebars only plays a minor role in the decrease of load-carrying capacity of composite girders. For the case where the corrosion of steel reinforcement is very important, the model in studies considering spatial pitting variability can be referenced (Han et al., 2019; Stewart, 2004)

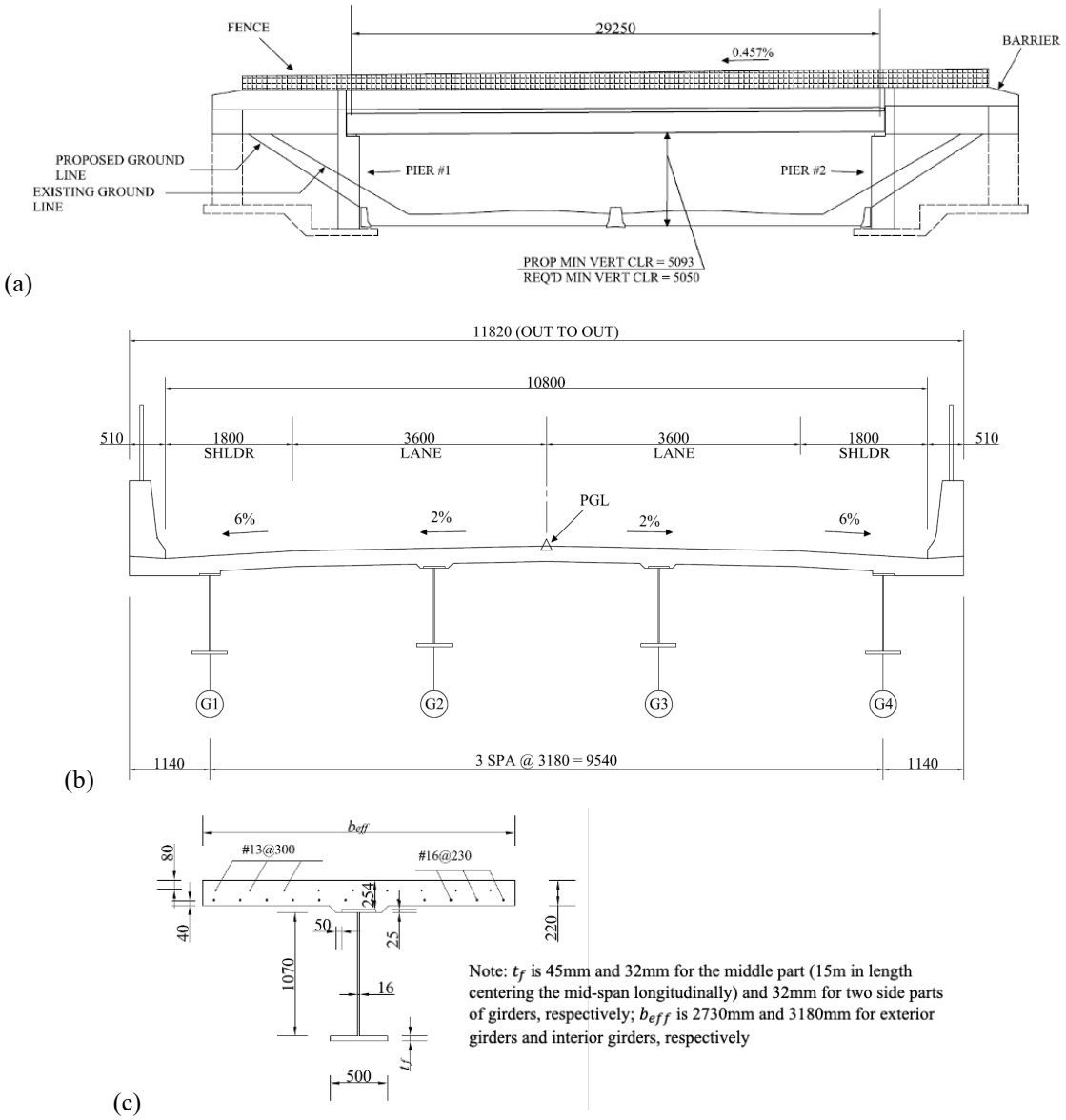

Figure 5.1 Schematic of Montgomery bridge: (a) elevation, (b) typical section, and (c) girder cross-section (all dimensions are in millimeters)

.Table 5.1 summarizes the random variables used to model uncertainties in flexural and shear capacities of composite girders as well as the corrosion process of deck reinforcement. Based on these random variables, Monte Carlo simulation with 10^5 samples was conducted to depict the time-variant uncertainties in structural capacities. The results of time-variant flexural capacities are shown in Figure 5.2 for an exterior girder made of carbon steel and A709-50CR, respectively. Similar results can be obtained for shear capacities. Five candidate distributions were used to fit the samples of structural capacities including Gumbel, Weibull, Gamma, lognormal, and normal distributions. AIC criteria (Akaike, 1998) were adopted to seek the best distribution to describe the uncertainties of load-carrying capacities. Normal distributions were found to be the best model for all shear and flexural capacities except for shear capacities of interior girders, in which case the normal distribution was the second-best model next to Weibull distribution.

Therefore, normal distributions were used to represent all flexural and shear capacities in reliability analysis.

Table 5.1 Random variables in the composite girder capacity calculations as well as the modeling of the corrosion process of deck reinforcement

Random Variable	Notation	Mean	COV	Distribution
Surface chloride content at deck (kg/m^3)[a]	C_0	3.5	0.5	Lognormal
Critical chloride content (kg/m^3)[a]	C_{cr}	0.9	0.19	Uniform[e]
Corrosion current density (μA/cm^2)[a]	i_{corr}	1.5	0.33	Uniform[f]
Chloride diffusion coefficient (mm^2/year)[a, b]	D_c	122.68	0.75	Lognormal
Height of concrete slab (mm)[c]	h_{slab}	220.8	0.016	Normal[g]
Bottom cover of transverse rebar in concrete (mm)[c]	C_{bot}	33.6	0.438	Normal[g]
Top cover of transverse rebar in concrete (mm)[c]	C_{top}	79.8	0.207	Normal[g]
Yield strength of steel rebar (MPa)[c]	f_{yr}	465.1	0.098	Normal[g]
Compressive strength of concrete (MPa)[c]	f_c	23.37	0.18	Normal[g]
Yield strength of carbon steel and A709-50CR[d]	f_y	379.5	0.11	Normal[g]
Corrosion rate of carbon steel (mm/year)	r_{corr}	0.067	1	Exponential
Corrosion rate ratio of A709-50CR to carbon steel	r_{ss}	0.014	0.378	Triangular[h]
Coating life (years)	t_0	15.4	0.344	Lognormal

Note: (a) Based on Stewart and Rosowsky (1998); (b) Based on Attard and Stewart (1999); (c) Based on Mirza and Macgregor (1979); (d) Based on Ellingwood et al. (1980); (e) The associated lower and upper bound of this uniform distribution is 0.6 and 1.2 kg/m^3, respectively; (f) The associated lower and upper bound of this uniform distribution is 1 and 2 μA/cm^2, respectively; (g) Normal distribution is assumed based on mean and COV; (h) The associated lower bound, mode, and upper bound are 0.001, 0.014, and 0.027, respectively.

Correlations between structural capacities were modeled based on assumptions stated in the previous section. Samples from Monte Carlo simulation were examined to determine the correlation coefficient between flexural and shear capacities of one girder as well as that among structural capacities of different girders. Example results of this analysis are shown in Figure 5.3 for flexural and shear capacities of an exterior girder at year 30. Because of the assumptions adopted, the correlation coefficients are also time-variant, as shown in Figure 5.4. Due to the lower corrosion rate, the correlation coefficient between structural capacities of A709-50CR girders does not vary significantly over time.

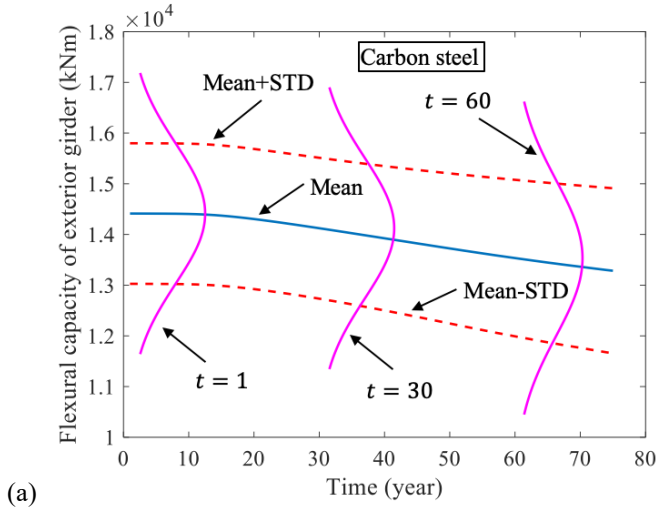

(a)

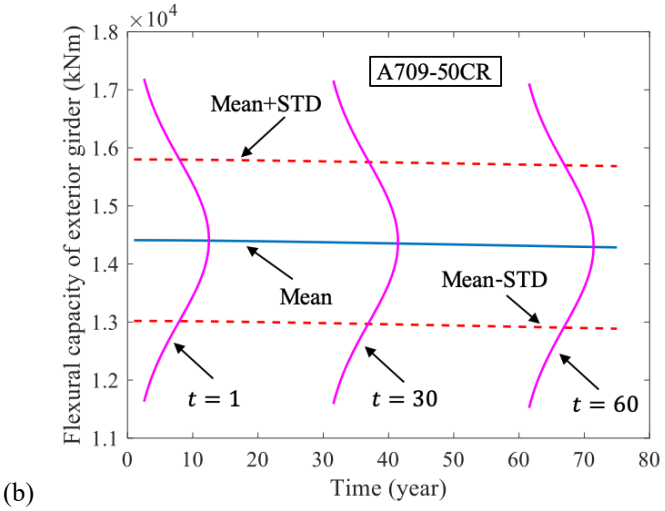

(b)

Figure 5.2 Time-variant flexural capacity of steel girders made of: (a) carbon steel and (b) A709-50CR

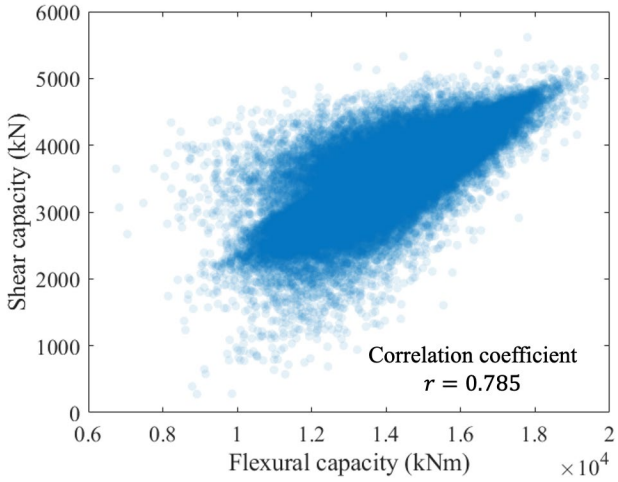

Figure 5.3 Correlation between flexural and shear capacities of the exterior girder at year 30

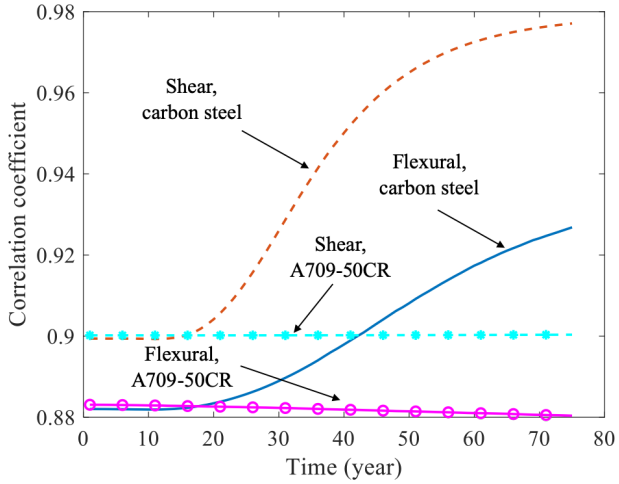

Figure 5.4 Time-variant correlation coefficient between structural capacities of exterior and interior girders

LOAD EFFECTS

For the case study bridge, dead load effects on an individual girder are determined based on the self-weight of the steel girder, the weight of the concrete slab and wearing surface within its tributary strip, and other miscellaneous weight (e.g., from steel fences and utilities) that are assumed to be distributed uniformly in the four girders.

The shear effects of exterior girders are controlled by one-lane traffic load. All other load effects are dictated by two-lane traffic load. For the simply supported bridge considered herein, the maximum bending moment in the mid-span section is obtained when the middle axle of the design truck is at the mid-span, and the maximum shear force is obtained when the rear axle of the design truck is near the support section. The girder distribution factors (GDFs) for bending moments are calculated based on Table 4.6.2.2.2b-1 and

Table 4.6.2.2.2d-1 in AASHTO (2017). The GDFs for shear forces are calculated according to Table 4.6.2.2.3a-1 and Table 4.6.2.2.3b-1 in AASHTO (2017). Existing studies suggest that the GDFs calculated based on AASHTO can be overconservative. The model error of GDFs associated with flexural failure mode can be inferred from existing load testing data (Eom & Nowak, 2001; Kim & Nowak, 1997; Nowak et al., 1998). The ratios of GDFs observed in these load tests to those calculated using AASHTO are calculated. Detailed information on the uncertainty of GDFs associated with flexural failure mode is shown in Table 5.2. Triangular distributions are assumed, and the corresponding parameters are regressed based on the calculated ratios. Since only flexural GDFs of interior girders are reliably reported in the selected load tests, it is assumed that the model error of flexural GDFs of interior girders are also applicable to exterior girders. For shear GDFs, the model error of shear GDFs for interior girders were obtained from the study by Suksawang et al. (2013). A uniform distribution was assumed for the model error distribution. For exterior girders, Barr and Amin (2006) compared the shear GDF obtained from lever rule with results of finite element modeling. The obtained ratio is used herein as the mean value of the model error. Unfortunately, only one data point is available from their study. It is therefore assumed that the coefficient of variation (COV) and the distribution type of shear GDFs for exterior girders are the same as those for interior girders. In summary, all variables relating to load effects as well as their corresponding uncertainties are listed in Table 5.3.

Table 5.2 Data used to quantify uncertainty of flexural GDFs

Bridge	GDF Obtained from Load Testing	GDF Calculated based on AASHTO	Model Error[d]	Reference
M50[a]	0.330	0.487	0.678	Kim and Nowak (1997)
	0.380		0.780	
	0.368		0.756	
	0.347		0.713	
US23[a]	0.428	0.542	0.790	
	0.427		0.788	
	0.447		0.825	
	0.455		0.840	
Bridge A[b]	0.265	0.434	0.611	Nowak et al. (1998)
	0.318		0.733	
	0.371		0.855	
	0.283		0.652	
Bridge B[b]	0.246	0.442	0.557	
	0.253		0.572	
	0.257		0.581	
Bridge C[b]	0.200	0.402	0.498	
	0.224		0.557	
	0.247		0.614	
	0.214		0.532	
	0.217		0.540	
	0.209		0.520	
Bridge D[b]	0.303	0.450	0.673	
	0.371		0.824	
	0.320		0.711	
Bridge E[b]	0.375	0.395	0.949	
	0.325		0.823	
	0.332		0.841	
Bridge 1[c]	0.38	0.44	0.864	Eom and Nowak (2001)
Bridge 2[c]	0.29	0.44	0.659	
Bridge 3[c]	0.27	0.40	0.675	
Bridge 4[c]	0.40	0.45	0.889	
Bridge 5[c]	0.36	0.40	0.900	
Bridge 6[c]	0.36	0.48	0.750	
Bridge 7[c]	0.52	0.53	0.981	
Bridge 8[c]	0.31	0.39	0.795	
Bridge 9[c]	0.69	0.68	1.015	
Bridge 10[c]	0.33	0.41	0.805	
Bridge 11[c]	0.32	0.43	0.744	
Bridge 12[c]	0.39	0.55	0.709	
Bridge 13[c]	0.39	0.51	0.765	
Bridge 14[c]	0.42	0.55	0.764	
Bridge 15*[c]	0.39	0.58	0.672	
Bridge 16*[c]	0.38	0.53	0.717	
Bridge 17*[c]	0.44	0.67	0.657	

Note: (a) Based on Kim and Nowak (1997); (b) Based on Nowak et al. (1998); (c) Based on Eom and Nowak (2001); (d) The model error herein refers to the ratio of load-testing GDF over AASHTO GDF.

Table 5.3 Variables relating to live load effects

Random Variable	Notation	Mean	COV	Distribution
Model uncertainty factor of the resistance of composite girder[a]	γ_{mg}	1.05	0.06	Normal[g]
Uncertainty factor associated with the weight of steel[a]	λ_{steel}	1.03	0.08	Normal[g]
Uncertainty factor associated with the weight of the concrete[a]	λ_{conc}	1.05	0.10	Normal[g]
Uncertainty factor associated with the wearing surface of the concrete[a]	$\lambda_{conc,w}$	1[f]	0.25	Normal[g]
Uncertainty factor associated with the miscellaneous items[a]	λ_{misc}	1.03	0.08	Normal[g]
Uncertainty factor associated with annual maximum moment induced by HL-93[a]	λ_{Ml}	1.20	0.19	Gumbel
Uncertainty factor associated with annual maximum shear of exterior girders induced by HL-93[a]	$\lambda_{Vl,ext}$	1.18	0.19	Gumbel
Uncertainty factor associated with annual maximum shear of interior girders induced by HL-93[a]	$\lambda_{Vl,int}$	1.18	0.19	Gumbel
GDF associated flexural live load effects of exterior girders[b]	$D_{f,ext}$	1.073	-	Deterministic
GDF associated flexural live load effects of interior girders[b]	$D_{f,int}$	1.076	-	Deterministic
GDF associated shear live load effects of exterior girders[b]	$D_{s,ext}$	0.713	-	Deterministic
GDF associated shear live load effects of interior girders[b]	$D_{s,int}$	0.981	-	Deterministic
Model error associated with GDFs of flexural live load effects[c]	λ_D	0.73	0.146	Triangular[h]
Model error associated with GDFs of shear live load effects of exterior girders[d]	$\lambda_{Ds,ext}$	1.02	0.060	Uniform[i]
Model error associated with GDFs of shear live load effects of interior girders[e]	$\lambda_{Ds,int}$	0.886	0.060	Uniform[j]
DLA of shear live load effect in exterior girders[a]	I_{g1}	0.15	0.8	Normal (assumed)
DLA of flexural live load effect and shear live load effect in interior girders[a]	I_g	0.10	0.8	Normal (assumed)

Note: (a) Based on Nowak (1999); (b) Calculated based on AASHTO (2017); (c) Based on Table 5.2; (d) Based on Barr and Amin (2006); (e) Based on Suksawang et al. (2013); (f) The mean value of $\lambda_{conc,w}$ is assumed to be 1; (g) Normal distribution is assumed based on mean and COV; (h) The associated lower bound, mode, and upper bound are 0.50,0.68, and 1.01, respectively; (i) The associated lower and upper bound are 0.915 and 1.125, respectively; (j) The associated lower and upper bound are 0.794 and 0.977, respectively.

Similar to the structural capacities, a number of assumptions were made to reflect the correlation between load effects within one girder and that between different girders. Since the two-lane traffic is in opposite directions, it was considered that the annual maximum bending moment in a composite girder is independent of the annual maximum shear force. Full correlation was assumed for the maximum bending moments in different girders, model error of flexural GDFs, and dynamic load allowance (DLA) for flexural

load effects. The same full-correlation assumption was adopted for interior girders in shear. For exterior girders in shear, the load effects and the associated GDFs and DLAs are independent from those for interior girders, since the former are controlled by one-lane traffic load.

RELIABILITY ANALYSIS AND RISK ASSESSMENT

Based on the AASHTO (2017) code, the performance functions associated with flexural failure can be expressed as

$$g_{gf,ext} = \gamma_{gf} R_{gf,ext}(t) - 435.23\lambda_{steel} - 2303.6\lambda_{conc} - 349.71\lambda_{conc,w} - 82.61\lambda_{misc} - 0.85 \cdot 2962.04\lambda_{Ml} \cdot \lambda_D D_{f,ext}(1 + I_g) \quad (5.1)$$

and

$$g_{gf,int} = \gamma_{gf} R_{gf,int}(t) - 435.23\lambda_{steel} - 2601.98\lambda_{conc} - 500.50\lambda_{conc,w} - 82.61\lambda_{misc} - 0.85 \cdot 2962.04\lambda_{Ml} \cdot \lambda_D D_{f,int}(1 + I_g) \quad (5.2)$$

for exterior and interior girders, respectively. In these functions, γ_{gf} is the model error associated with the AASHTO model for flexural capacities; $R_{gf,ext}(t)$ and $R_{gf,int}(t)$ are the time-variant flexural capacities of an exterior girder and an interior girder, respectively; λ_{steel}, λ_{conc}, $\lambda_{conc,w}$, and λ_{misc} are the uncertainty factors for dead load effects due to steel, concrete deck, wearing surface, and miscellaneous items, respectively; λ_{Ml} is the uncertainty factor of the live load moment due to HL-93; $D_{f,ext}$ and $D_{f,int}$ are the calculated GDFs for bending moments; λ_D represents the model errors of the flexural GDFs; and I_g is the DLA. The factor 0.85 is used to account for the fact that when two-lane traffic load controls, the maximum traffic load in each lane should be lower than that in the one-lane control case (Nowak, 1999).

Similarly, the performance functions associated with shear failure are

$$g_{gs,ext} = \gamma_{gs} R_{gs,ext}(t) - 59.25\lambda_{steel} - 315.02\lambda_{conc} - 47.82\lambda_{conc,w} - 11.26\lambda_{misc} - 1.0 \cdot 425.09\lambda_{Vl,ext} \cdot \lambda_{Ds,ext} D_{s,ext}(1 + I_{g1}) \quad (5.3)$$

for exterior girders and

$$g_{gs,int} = \gamma_{gs} R_{gs,int}(t) - 59.25\lambda_{steel} - 355.83\lambda_{conc} - 68.45\lambda_{conc,w} - 11.26\lambda_{misc} - 0.85 \cdot 425.09\lambda_{Vl,int} \cdot \lambda_{Ds,int} D_{s,int}(1 + I_g) \quad (5.4)$$

for interior girders, where γ_{gs} is the model error associated with the AASHTO model for shear capacities; $R_{gs,ext}(t)$ and $R_{gs,int}(t)$ are the time-variant shear capacities of an exterior girder and an interior girder, respectively; $\lambda_{Vl,ext}$ and $\lambda_{Vl,int}$ are the uncertainty factors associated with the HL-93 induced shear force in exterior girders (controlled by one-lane traffic load) and interior girders (controlled by two-lane traffic load), respectively; $D_{s,ext}$ and $D_{s,int}$ are the calculated GDFs for shear forces in exterior girders and interior girders, respectively; $\lambda_{Ds,ext}$ and $\lambda_{Ds,int}$ are the uncertainty factors associated with the GDFs of the traffic-induced shear forces in exterior and interior girders, respectively; and I_{g1} is the DLA associated with the shear load effects in exterior girders (induced by one-lane load).

Based on the system model in Figure 4.1, the failure of the bridge superstructure is considered herein due to the failure of two adjacent girders. Using FORM for component reliability analysis, the annual reliability

index profiles associated with the flexural and shear failures are shown in Figure 5.5. Girders made of carbon steel and A709-50CR are analyzed separately and shown in Figure 5.5(a) and Figure 5.5(b), respectively. Since the corrosion rate of A709-50CR is extremely small, the decrease in annual reliability indices is negligible. Based on the approach for system reliability analysis, Figure 5.6 shows the results of annual system reliability indices for bridges made of carbon steel and A709-50CR. To translate the time-variant reliability to lifecycle risk, consequence parameters used in Eqs. (4.10) through (4.12) are provided in Table 5.4. It should be noted that the bridge failure can affect traffic both on and beneath the bridge. Therefore, Eqs. (4.11) and (4.12) should be used twice to determine the total indirect cost. The annual risk values are presented in Figure 5.6 for bridges made of carbon steel and A709-50CR. Based on the annual risks, the lifecycle risk of bridge failure can be calculated. Figure 5.5 and Figure 5.6 show that A709-50CR can effectively enhance the lifetime reliability of steel bridges and mitigate the lifecycle failure risk. In the following subsection, the benefit of using A709-50CR for maintenance is investigated based on the case study bridge originally made of carbon steel.

Table 5.4 Variables for cost and consequence evaluation

Variable	Notation	Mean	COV	Distribution
ADT on the bridge[a]	-	1935	-	Deterministic
Ratio of ADTT to ADT on the bridge[a]	-	0.08	-	Deterministic
ADT beneath the bridge[a]	-	26371	-	Deterministic
ADTT/ADT ratio beneath the bridge[a]	-	0.04	-	Deterministic
Detour length on the bridge (km)[a]	-	3.22	-	Deterministic
Detour length beneath the bridge (km)[a]	-	4.83km	-	Deterministic
Average compensation to truck drivers (USD/h)[b]	C_{ATC}	26.97	0.15	Lognormal
Average wage of car drivers (USD/h)[b]	C_{AW}	22.82	0.15	Lognormal
Average detour speed (km/h)[c]	S	50	0.15	Lognormal
Average vehicle occupancies for cars[c]	O_{Car}	1.5	0.15	Lognormal
Average vehicle occupancies for trucks[c]	O_{truck}	1.05	0.15	Lognormal
Running cost of cars (USD/km)[c]	$c_{Run,car}$	0.08	0.20	Lognormal
Running cost of trucks (USD/km)[c]	$c_{Run,truck}$	0.375	0.20	Lognormal
Time value of a cargo (USD/h)[c]	c_{goods}	4	0.20	Lognormal
Rebuilding cost (USD/m^2)[d]	$R_{Reb,0}$	1,086,500	-	Deterministic
Repair cost of a girder (USD)[d]	C_{rep}	216,400	-	Deterministic
Discount rate	r	2%	-	Deterministic

Note: (a) Based on NBI (FHWA, 1992); (b) Based on AASHTO (2010); (c) Based on Deco and Frangopol (2011); (d) Based on Estes and Frangopol (1999).

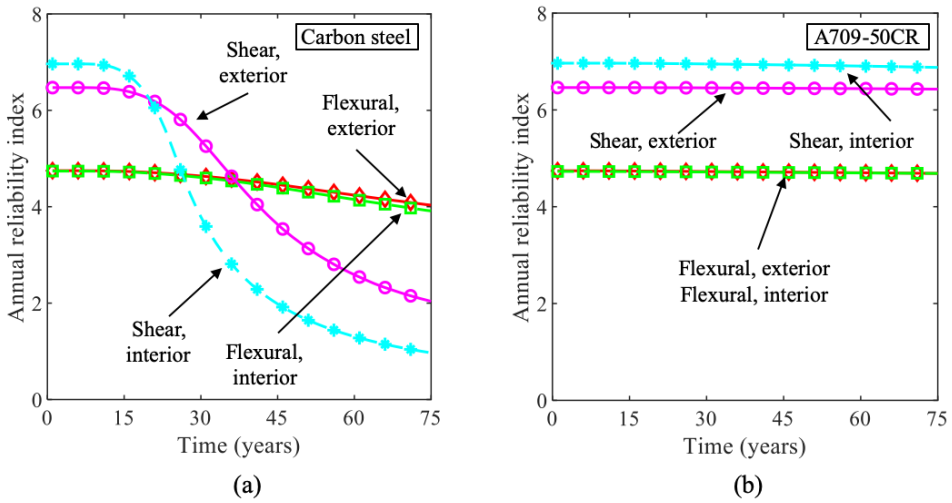

Figure 5.5 Annual reliability index profiles associated with individual failure modes: (a) carbon steel girder and (b) A709-50CR girder

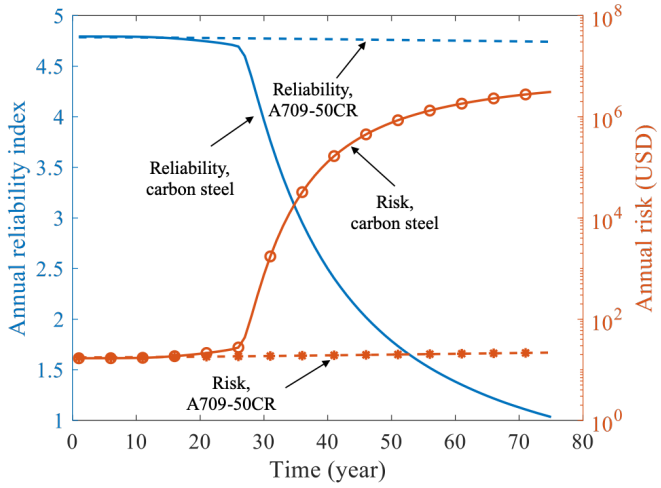

Figure 5.6 Annual reliability and risk profiles of the superstructure

RESULTS OF LIFECYCLE MAINTENANCE OPTIMIZATION

The bi-objective optimization, as introduced in Chapter 4, is carried out to optimize maintenance plans that can minimize the lifecycle risk and the lifecycle maintenance cost. Herein, major maintenance actions in the form of girder replacement are considered. To investigate the benefit of using A709-50CR for maintenance, two maintenance scenarios are considered. In the first scenario, girder replacement is carried out using the same carbon steel material. Under this condition, the bridge after maintenance may again suffer from corrosion once the protective coating breaks down. In the second scenario, A709-50CR girders are used for girder replacement. It is of interest to investigate whether the excellent corrosion resistance of A709-50CR can bring in lifecycle cost savings.

Data in Table 5.4 are used to calculate the maintenance costs using carbon steel and A709-50CR girders as well as the failure consequences. Based on the material cost data, the initial cost of one A709-50CR girder

is 7.9% higher than that of a carbon steel girder. Considering the potential volatility of A709-50CR cost, three additional cases are analyzed where the cost of an A709-50CR girder is assumed to be 20%, 50%, and 100% higher than that of a carbon steel girder. In addition to maintenance cost, the target reliability index can also significantly affect the optimal maintenance plan. Therefore, two reliability levels (i.e., $\beta_{thr,i}$ = 2.0 and $\beta_{thr,i}$ = 3.5, where $i = 1,2,\dots,N$) are used separately as a constraint in the optimization problem. In the former case, the maximum number of maintenance actions for one girder is 3 for carbon steel and 1 for A709-50CR; in the latter case, the number is 4 for carbon steel and 1 for A709-50CR. To solve the optimization problem using NSGA-II, the population size of one generation is 1,000; the maximum generation and maximum stall generation are 1,000 and 100, respectively. Adaptive Gaussian mutation and scattered crossover are adopted within each generation (MathWorks, 2018).

The results of a bi-objective optimization can be presented on a Pareto front (Pareto, 2014). Maintenance plans on the Pareto front are tradeoffs between two competing objectives; i.e., one cannot improve one objective without sacrificing the quality of the second objective. Figure 5.7 shows the Pareto fronts associated with $\beta_{thr,i}$ = 2.0 ($i = 1,2,\dots N$) and different costs. As the cost of A709-50CR girders increases, the Pareto front associated with using carbon steel intersects with the Pareto fronts of Cases II, III, and IV. This means that (a) using carbon steel for girder replacement is the cheaper option when the acceptable lifecycle risk is higher than 11,300 USD, and (b) as the risk requirement is more stringent, the advantage of using A709-50CR becomes more salient (as shown in Figure 5.7 (b)). This can be further demonstrated by the Pareto fronts for the case where $\beta_{thr,i}$ = 3.5 ($i = 1,2,\dots N$), as shown in Figure 5.8. In this case, using A709-50CR can be more cost-effective in achieving the required threshold of lifecycle risk. For instance, when the risk threshold is 1,000 USD, the associated lifecycle maintenance cost of using A709-50CR is about 42,000 USD, given cost data provided by ArcelorMittal (Case II), about 20% lower than that of using carbon steel (Case I). The comparative advantage of using A709-50CR is significant even when the cost of a A709-50CR girder is raised to 1.2 times the cost of a carbon steel girder (Case III). Overall, for both $\beta_{thr,i}$ = 2.0 and $\beta_{thr,i}$ = 3.5, using A709-50CR for maintenance can save lifecycle cost when the safety requirement is strict, and this advantage exists as long as the cost of A709-50CR girders is below 1.5 times the cost of carbon steel girders.

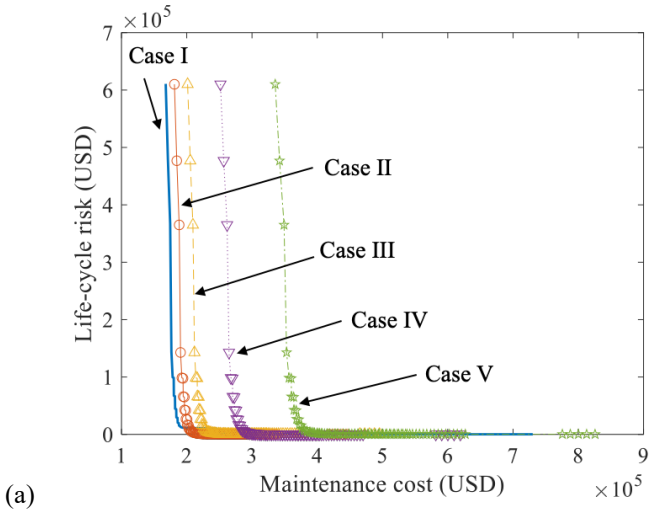

(a)

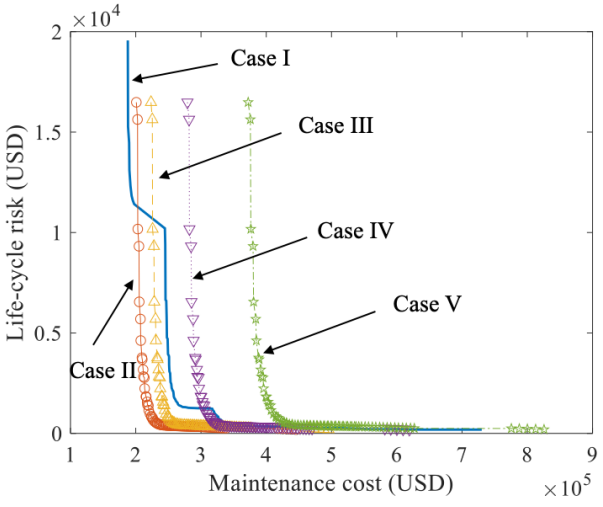

(b)

Note: Case I = carbon steel; Case II = A709-50CR (market cost); Case III = A709-50CR (cost assumed to be 1.2 times that of carbon steel); Case IV = A709-50CR (cost assumed to be 1.5 times that of carbon steel); Case V = A709-50CR (cost assumed to be 2.0 times that of carbon steel)

Figure 5.7 Optimal Pareto front under reliability constraint $\beta_{thr,I}$ = 2.0: (a) considering all lifecycle risk values and (b) lifecycle risk is lower than 20,000 USD

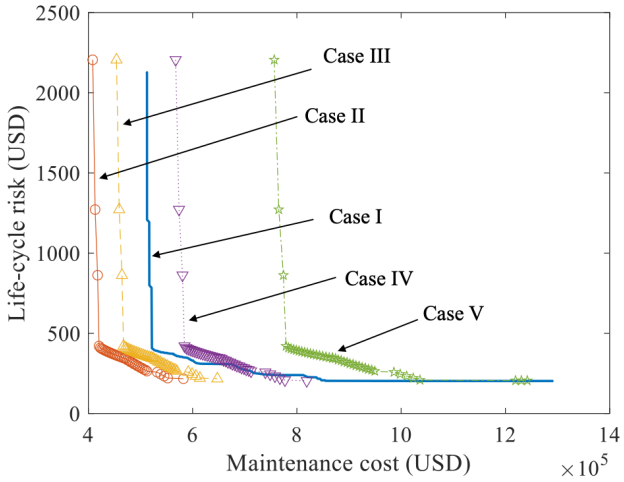

Note: Case I = carbon steel; Case II = A709-50CR (market cost); Case III = A709-50CR (cost assumed to be 1.2 times that of carbon steel); Case IV = A709-50CR (cost assumed to be 1.5 times that of carbon steel); Case V = A709-50CR (cost assumed to be 2.0 times that of carbon steel)

Figure 5.8 Optimal Pareto front under reliability constraint $\beta_{thr,I} = 3.5$

CHAPTER 6

Conclusions

CONCLUSIONS

As a representative high-performance construction material, a new type of corrosion-resistant steel, namely A709-50CR, is investigated for its lifecycle environmental impacts and the potential to be used in lifecycle maintenance actions. The corrosion-resistance properties of A709-50CR are quantified based on an extensive literature review. The lifecycle environmental impacts are assessed based on international standards while considering uncertainties involved in the input inventory data. For lifecycle maintenance optimization, a risk-based approach was adopted. In particular, given the corrosion rate of carbon steel and A709-50CR, the annual risk profiles of a multi-girder bridge consisting of carbon steel and A709-50CR steel can be determined. Optimization was then performed to obtain optimal solutions associated with using carbon steel and A709-50CR for girder replacement. This is the first study to investigate the application of A709-50CR in the maintenance planning of existing bridges subjected to corrosion. The following conclusions are drawn:

(1) Based on the literature review on the corrosion behavior of A709-50CR and other types of martensitic stainless steel with similar chemical composition, it was found that the corrosion rate of A709-50CR is much lower than that of carbon steel when exposed to the same type of environment. For bridges under atmospheric corrosion in a marine environment, the corrosion rate of A709-50CR is about 0.1-2.7% of that of carbon steel. The high corrosion resistance of A709-50CR indicates no painting/repainting and other corrosion-related maintenance actions are needed for A709-50CR girders.

(2) Lifecycle inventory analysis indicates that when used as bridge girders, the initial CO_2, SO_2, and NO_x emissions of A709-50CR are higher than those associated with carbon steel girders. However, the total lifecycle CO_2 and NO_x emissions of A709-50CR girders are significantly lower than those associated with carbon steel girders. The lifecycle SO_2 emissions of A709-50CR girders are comparable to those associated with carbon steel girders due to the potentially high SO_2 emissions in the production phase of A709-50CR.

(3) Based on the lifecycle inventory results, the lifecycle environmental impact analysis concludes that the initial global warming potential, acidification potential, and eutrophication potential of A709-50CR girders can be higher than those associated with carbon steel girders. However, the total lifecycle GWP, AP, and EP of A709-50CR girders are significantly lower than those associated with carbon steel girders. The breakeven time for GWP and EP of A709-50CR girders will happen at about 15 years in service, usually right after one repainting action. The AP of A709-50CR girders is likely to reach its breakeven point within 20 to 60 years after construction (i.e., after one or two repainting actions).

(4) Due to corrosion, a bridge may need multiple girder replacement actions in its service life. A709-50CR, when used in replacement girders, can effectively reduce the number of major maintenance actions. Therefore, using A709-50CR to replace corroded girders can be significantly cost-effective compared with using carbon steel. The exact cost-effectiveness depends on the cost ratio of A709-

50CR over carbon steel and the acceptable lifecycle risk (or similarly the reliability threshold on girders).

(5) When the acceptable lifecycle risk is low (or the reliability threshold is high), using A709-50CR for girder replacement can yield lower lifecycle cost. This comparative advantage is significant based on the market data of A709-50CR and carbon steel costs and can still be pronounced even when the cost of a A709-50CR girder is about 50% higher than that of carbon steel. When the cost of A709-50CR is even higher, the cost-effectiveness of using A709-50CR for girder replacement starts to diminish. Similarly, when the acceptable lifecycle risk is high (or the reliability threshold is low), carbon steel becomes cheaper than A709-50CR for girder replacement.

(6) To provide more accurate predictions on lifecycle cost and performance of steel bridges, future research is still needed to reduce the uncertainties associated with the corrosion rate of carbon steel and the corrosion rate ratio of A709-50CR to carbon steel. Due to galvanic corrosion at the interface between carbon steel and A709-50CR, caution should be taken when using A709-50CR in existing carbon steel bridges. This corrosion mechanism can be mitigated by detailing measures such as adding nonmetallic filler plates.

ACKNOWLEDGEMENTS

The authors are grateful for the financial support received from the U.S. Department of Transportation Region 3 University Transportation Center (Grant CIAM-UTC-REG6). The opinions and conclusions presented in this report are those of the authors and do not necessarily reflect the views of the sponsoring organization. The authors would also like to thank Mr. Thomas P. Macioce, P.E., from the Pennsylvania Department of Transportation for providing the bridge drawings used in the case study, and Dr. Fred B. Fletcher from ArcelorMittal Global R&D for information relating to A709-50CR. Mr. Trystan Golden, undergraduate student at Lehigh University, helped with the analysis of coating life inferred from NBI data. Mr. Cheng Yuan, graduate student at Lehigh University, conducted the lifecycle environmental assessment for A709-50CR and conventional carbon steel girders. Their help is herein acknowledged.

References

AASHTO. (2010). *User and Non-user Benefit Analysis for Highways*. American Association of State Highway and Transportation Officials (AASHTO).

AASHTO. (2017). *AASHTO LRFD Design Specifications*. American Association of State Highway and Transportation Officials (AASHTO).

Akaike, H. (1998). Information theory and an extension of the maximum likelihood principle. In *Selected Papers of Hirotugu Akaike* (pp. 199–213). Springer.

Akgül, F. (2002). *Lifetime System Reliability Prediction for Multiple Structure Types in a Bridge Network*. University of Colorado Boulder.

Albrecht, P., & Hall Jr., T. T. (2003). Atmospheric corrosion resistance of structural steels. *Journal of Materials in Civil Engineering*, *15*(1), 2–24. https://doi.org/10.1061/(ASCE)0899-1561(2003)15

Albrecht, P., & Naeemi, A. H. (1984). *Performance of Weathering Steel in Bridges*. NCHRP Report 272. Transportation Research Board.

Ang, A. H.-S., & Tang, W. H. (1984). *Probabilistic Concepts in Engineering Planning and Design, Vol. 2*. John Wiley & Sons Inc.

Ang, A. H.-S., & Tang, W. H. (2007). *Probability Concepts in Engineering Planning and Design: Emphasis on Application to Civil and Environmental Engineering*. Wiley.

ASCE. (2017). *Report Card for America's Infrastructure*. American Society of Civil Engineers (ASCE).

ASTM Committee B-3. (1959). Larrabee, C. P., and Ellis, O. B. Report of subgroup of subcommittee VI on corrosiveness of various atmospheric test sites as measured by specimens of steel and zinc. In *Proceedings of ASTM, 59* (pp. 183–201). American Society for Testing and Materials (ASTM).

Attard, M. M., & Stewart, M. G. (1999). A two-parameter stress block for high-strength concrete. *ACI Structural Journal*, *95*(3), 305–317.

Barone, G., & Frangopol, D. M. (2014a). Reliability, risk and lifetime distributions as performance indicators for life-cycle maintenance of deteriorating structures. *Reliability Engineering and System Safety*, *123*, 21–37. https://doi.org/10.1016/j.ress.2013.09.013

Barone, G., & Frangopol, D. M. (2014b). Life-cycle maintenance of deteriorating structures by multi-objective optimization involving reliability, risk, availability, hazard and cost. *Structural Safety*, *48*, 40–50. https://doi.org/10.1016/j.strusafe.2014.02.002

Barr, P. J., & Amin, M. N. (2006). Shear live-load distribution factors for I-girder bridges. *Journal of Bridge Engineering*, *11*(2), 197–204. https://doi.org/10.1061/(ASCE)1084-0702(2006)11

Chun, J., Song, J., & Paulino, G. H. (2015). Parameter sensitivity of system reliability using sequential compounding method. *Structural Safety*, *55*, 26–36. https://doi.org/10.1016/j.strusafe.2015.02.001

Cobb, H. M. (1999). *Steel Products Manual - Stainless Steels*. Iron and Steel Society.

Copson, H. R. (1960). Long-time atmospheric corrosion tests on low-alloy steels. In *Proceedings of ASTM, 60* (pp. 650–666). American Society for Testing and Materials (ASTM).

Daghash, S. M., & Ozbulut, O. E. (2017). Mechanical evaluation of corrosion-resistant steel plates for bridge girder fabrication. *Structures Congress*, 494–505.

Deb, K., Pratap, A., Agarwal, S., & Meyarivan, T. (2002). A fast and elitist multiobjective genetic algorithm: NSGA-II. *IEEE Transactions on Evolutionary Computation*, *6*(2), 182–197. https://doi.org/10.1109/4235.996017

Decò, A., & Frangopol, D. M. (2011). Risk assessment of highway bridges under multiple hazards. *Journal of Risk Research*, *14*(9), 1057–1089. https://doi.org/10.1080/13669877.2011.571789

Díaz, I., Cano, H., Chico, B., De La Fuente, D., & Morcillo, M. (2012). Some clarifications regarding literature on atmospheric corrosion of weathering steels. *International Journal of Corrosion*, *i*. https://doi.org/10.1155/2012/812192

Ditlevsen, O. (1979). Narrow reliability bounds for structural systems. *Journal of Structural Mechanics*, *7*(4), 453–472. https://doi.org/10.1080/03601217908905329

Ebrahimi, N., Zhang, J., Baldock, B., & Lai, D. (2018). Galvanic corrosion risk assessment of bolt materials in ASTM A1010 steel bridges. *Corrosion Conference and Expo 2018*.

Ellingwood, B., Galambos, T. V., MacGregor, J. G., & Cornell, C. A. (1980). *Development of a Probability Based Load Criterion for American National Standard A58,* Report 577. National Bureau of Standards (NBS).

Enright, M. P., & Frangopol, D. M. (1998). Probabilistic analysis of resistance degradation of reinforced concrete bridge beams under corrosion. *Engineering Structures*, *20*(11), 960–971. https://doi.org/10.1016/S0141-0296(97)00190-9

Eom, J., & Nowak, A. S. (2001). Live load distribution for steel girder bridges. *Journal of Bridge Engineering*, *6*(6), 489–497. https://doi.org/10.1061/(ASCE)1084-0702(2001)6:6(489)

Estes, A. C. (1997). *A System Reliability Approach to the Lifetime Optimization of Inspection and Repair of Highway Bridges*. University of Colorado Boulder.

Estes, A. C., & Frangopol, D. M. (1999). Repair optimization of highway bridges using system reliability approach. *Journal of Structural Engineering, ASCE*, *125*(7), 766–775.

FHWA. (1992). *National Bridge Inventory (NBI)*. Federal Highway Administration Website. https://www.fhwa.dot.gov/bridge/nbi.cfm

FHWA. (2011). *Improved Corrosion-Resistant Steel for Highway Bridge Construction (FHWA-HRT-11-061)*. Federal Highway Administration (FHWA).

Fiorillo, G., & Ghosn, M. (2019). Risk-based importance factors for bridge networks under highway traffic loads. *Structure and Infrastructure Engineering*, *15*(1), 113–126. https://doi.org/10.1080/15732479.2018.1496119

Gallivan, F., Ang-Olson, J., Papson, A., & Venner, M. (2010). *Greenhouse Gas Mitigation Measures for Transportation Construction, Maintenance, and Operations Activities*. Transportation Research Board.

Genz, A. (1992). Numerical computation of multivariate normal probabilities. *Journal of Computational and Graphical Statistics*, *1*(2), 141–149.

Gervásio, H., da Silva, L. S., Perdigão, V., Orcesi, A., & Andersen, R. (2015). Influence of maintenance strategies on the life cycle performance of composite highway bridges. *Structural Engineering International*, *25*(2), 184–196. https://doi.org/10.2749/101686614X14043795569978

GHK/BioIS. (2006). *Costs and Benefits of the ELV Directive – Final Report*. GHK/BioIS.

Gollwitzer, S., & Rackwitz, R. (1983). Equivalent components in first-order system reliability. *Reliability Engineering*, *5*(2), 99–115.

Gouda, V. K., Shater, M. A., & Mikhail, R. S. (1975). Hardened Portland blast-furnace slag cement pastes II. The corrosion behavior of steel reinforcement. *Cement and Concrete Research*, *5*, 1–13. https://doi.org/10.1016/0008-8846(75)90103-9

Groshek, I. G. (2017). *Corrosion Behavior of ASTM A1010 Stainless Steel for Applications in Bridge Components*. Virginia Polytechnic Institute and State University.

Han, X., Yang, D. Y., & Frangopol, D. M. (2019). Time-variant reliability analysis of steel plates in marine environments considering pit nucleation and propagation. *Probabilistic Engineering Mechanics*, *57*, 32–42. https://doi.org/10.1016/j.probengmech.2019.05.003

Heijungs, R. (1992). *Environmental Life-cycle Assessment of Products*. Centre of Environmental Science.

Hohenbichler, M., & Rackwitz, R. (1983). First-order concepts in system reliability. *Structural Safety*, *1*, 177–188.

Hohenbichler, M., & Rackwitz, R. (1986). Sensitivity and importance measures in structural reliability. *Civil Engineering Systems*, *3*(12), 203–209. https://doi.org/10.1080/02630258608970445

International Energy Agency. (2019). *CO2 Emissions from Fuel Combustion: Database Documentation*. International Energy Agency.

ISO 14040. (2006). *Environmental Management — Life Cycle Assessment — Principles and Framework*. International Organization for Standardization (ISO).

ISO 14044. (2006). *Environmental Management — Life Cycle Assessment — Requirements and Guidelines*. International Organization for Standardization (ISO).

ISSF. (2019). *Stainless Steel and CO2: Facts and Scientific Obsrvations*. International Stainless Steel Forum (ISSF).

Jolliet, O., Margni, M., Charles, R., Humbert, S., Payet, J., Rebitzer, G., & Rosenbaum, R. (2003). IMPACT 2002+: A new life cycle impact assessment methodology. *The International Journal of Life Cycle Assessment*, *8*(6), 324–330. https://doi.org/10.1007/BF02978505

Karl, T., & Koss, W. J. (1984). Regional and national monthly, seasonal, and annual temperature weighted by area, 1895-1983. *National Climatic Data Center*.

Kim, S., & Nowak, A. S. (1997). Load distribution and impact factors for I-girder bridges. *Journal of Bridge Engineering*, *2*(3), 97–104. https://doi.org/10.1061/(ASCE)1084-0702(1997)2:3(97)

Kim, T., & Chae, C. (2016). Environmental impact analysis of acidification and eutrophication due to emissions from the production of concrete. *Sustainability*, *8*(6), 578. https://doi.org/10.3390/su8060578

Knotkova, D., Kreislova, K., & Dean, Jr., S. W. (2012). *International Atmospheric Exposure Program: Summary of Results*. American Society for Testing and Materials (ASTM).

Kogler, R. (2015). *Steel Bridge Design Handbook: Corrosion Protection of Steel Bridges* (Vol. 19, Issue December). Federal Highway Administration (FHWA).

Kucera, V., & Mattsson, E. M. (1982). Atmospheric corrosion of Bimetallic Structures. In *Atmospheric Corrosion*. Wiley.

MathWorks. (2018). *Global Optimization Toolbox User's Guide*. The MathWorks.

Melchers, R. E. (2007). Transition from marine immersion to coastal atmospheric corrosion for structural steels. *Corrosion*, *63*(6), 500–514. https://doi.org/10.5006/1.3278401

Mirza, S. A., & MacGregor, J. G. (1979). Variations in dimensions of reinforced concrete members. *Journal of the Structural Division*, *105*(4), 751–766.

Morcillo, M., Simancas, J., & Feliu, S. (1995). Long-term atmospheric corrosion in Spain: Results after 13-16 years of exposure and comparision with worldwide data. In *Atmospheric Corrosion: ASTM STP 1239* (pp. 195–214). American Society for Testing and Materials (ASTM).

NACE International. (2012). *Corrosion Control Plan for Bridges*. National Association of Corrosion Engineers (NACE).

Norgate, T. E., Jahanshahi, S., & Rankin, W. J. (2004). Alternative routes to stainless steel - A life cycle approach. *Proceedings of the Tenth International Ferroalloys Congress*.

Norgate, T. E., Jahanshahi, S., & Rankin, W. J. (2007). Assessing the environmental impact of metal production processes. *Journal of Cleaner Production*, *15*(8–9), 838–848. https://doi.org/10.1016/j.jclepro.2006.06.018

Nowak, A S. (1999). Calibration of LRFD Bridge Design Code. In *Report 368*. Transportation Research Board.

Nowak, A. S., Eom, J., Sanli, A., & Till, R. (1998). Verification of girder-distribution factors for short-span steel girder bridges by field testing. *Transportation Research Record*, *1*(99), 62–67.

Okasha, N. M., Frangopol, D. M., Fletcher, F. B., & Wilson, A. D. (2012). Life-cycle cost analyses of a new steel for bridges. *Journal of Bridge Engineering*, *17*(1), 168–172. https://doi.org/10.1061/(ASCE)BE

Pareto, V. (2014). *Manual of Political Economy*. Oxford University Press.

Provines, J. T., Sharp, S. R., Ozbulut, O., & Daghash, S. (2019). *Maintenance-Free Corrosion-Resistant Steel Plate for Bridges*. Virginia Transportation Research Council, Final Report VTRC 19-R21.

Sabatino, S., Frangopol, D. M., & Dong, Y. (2015). Sustainability-informed maintenance optimization of highway bridges considering multi-attribute utility and risk attitude. *Engineering Structures*, *102*, 310–321. https://doi.org/10.1016/j.engstruct.2015.07.030

SAE J2334. (1998). *Cosmetic Corrosion Lab Test*. SAE International.

Schmitt, R. J., & Mullen, C. X. (1968). Influence of chromium on the atmospheric-corrosion behavior of steel. In *Stainless Steel for Architecture Use: STP 454* (pp. 124–136). American Society for Testing and Materials (ASTM).

Soliman, M., & Frangopol, D. M. (2015). Life-cycle cost evaluation of conventional and corrosion-resistant steel for bridges. *Journal of Bridge Engineering, ASCE*, *20*(1), 06014005. https://doi.org/10.1061/(ASCE)BE.1943-5592.0000647.

Southwell, C. R., & Bultman, J. D. (1975). *Corrosion of Metals in Tropical Environments: Final Report of 16-year Exposure*. Naval Research Laboratory.

Stewart, M. G. (2004). Spatial variability of pitting corrosion and its influence on structural fragility and reliability of RC beams in flexure. *Structural Safety*, *26*(4), 453–470. https://doi.org/10.1016/j.strusafe.2004.03.002

Stewart, M. G., & Rosowsky, D. (1998). Time-dependent reliability of deteriorating reinforced concrete bridge decks. *Structural Safety*, *20*(1), 91–109. https://doi.org/10.1016/S0167-4730(97)00021-0

Suksawang, N., Nassif, H., & Su, D. (2013). Verification of shear live-load distribution factor equations for I-girder bridges. *KSCE Journal of Civil Engineering*, *17*(3), 550–555. https://doi.org/10.1007/s12205-013-0607-3

The Swedish Transport Administration. (2016). *Environmental Product Declaration for Railway Bridges on the Bothnia Line*. The Swedish Transport Administration.

Thoft-Christensen, P., Jensen, F. M., Middleton, C. R., & Blackmore, A. (1996). Assessment of the reliability of concrete slab bridges. *7th IFIP WG7.5 Working Conference on Reliability and Optimization of Structural Systems*.

Turconi, R., Boldrin, A., & Astrup, T. (2013). Life cycle assessment (LCA) of electricity generation technologies: Overview, comparability and limitations. *Renewable and Sustainable Energy Reviews*, *28*, 555–565. https://doi.org/10.1016/j.rser.2013.08.013

US Environmental Protection Agency. (2006). *Emission Factor Documentation: Iron and Steel Production*. United States Environmental Protection Agency.

Val, D. V., & Melchers, R. E. (1997). Reliability of deterioration RC slab Bridges. *Journal of Structural Engineering*, *123*(12), 1638–1644. https://doi.org/10.1061/(ASCE)0733-9445(1997)123:12(1638)

Valspar Industrial Mix. (2016). *Technical Data Sheet: FP402 Zinc Rich Epoxy Primer Grey*.

W. Kirchstetter, T., Harley, R. A., Kreisberg, N. M., Stolzenburg, M. R., & Hering, S. V. (1999). On-road measurement of fine particle and nitrogen oxide emissions from light- and heavy-duty motor vehicles. *Atmospheric Environment*, *33*(18), 2955–2968. https://doi.org/10.1016/S1352-2310(99)00089-8

Wang, X. Q., Tao, Z., Song, T. Y., & Han, L. H. (2014). Stress-strain model of austenitic stainless steel after exposure to elevated temperatures. *Journal of Constructional Steel Research*, *99*, 129–139. https://doi.org/10.1016/j.jcsr.2014.04.020

Wang, Z., Yang, D. Y., Frangopol, D. M., & Jin, W. (2019). Inclusion of environmental impacts in life-cycle cost analysis of bridge structures. *Sustainable and Resilient Infrastructure*, 5:4, 252-267, https://doi.org/10.1080/23789689.2018.1542212

Wright, R. (1980). Toughness of ferritic stainless steels. In *Toughness of Ferritic Stainless Steels - ASTM STP 706* (pp. 2–33). American Society for Testing and Materials (ASTM). https://doi.org/10.1520/stp38200s

Yang, D. Y., Frangopol, D. M., & Teng, J.-G. (2019). Probabilistic life-cycle optimization of durability-enhancing maintenance actions: Application to FRP strengthening planning. *Engineering Structures*, *188*, 340–349. https://doi.org/10.1016/j.engstruct.2019.02.055